

Rowan University

Rowan Digital Works

Theses and Dissertations

7-1-2020

Remediation of desiccation cracking in clayey soils through bio-cementation and bottom ash

Mark Vail
Rowan University

Follow this and additional works at: <https://rdw.rowan.edu/etd>



Part of the Geotechnical Engineering Commons

Let us know how access to this document benefits you - share your thoughts on our feedback form.

Recommended Citation

Vail, Mark, "Remediation of desiccation cracking in clayey soils through bio-cementation and bottom ash" (2020). *Theses and Dissertations*. 2829.

<https://rdw.rowan.edu/etd/2829>

This Thesis is brought to you for free and open access by Rowan Digital Works. It has been accepted for inclusion in Theses and Dissertations by an authorized administrator of Rowan Digital Works. For more information, please contact LibraryTheses@rowan.edu.

**REMEDICATION OF DESICCATION CRACKING IN CLAYEY SOILS
THROUGH BIO-CEMENTATION AND BOTTOM ASH ADMIXTURE**

by

Mark Vail

A Thesis

Submitted to the
Department of Civil and Environmental Engineering
College of Engineering

In partial fulfillment of the requirement
For the degree of

Master of Science in Civil and Environmental Engineering
at

Rowan University

June 5, 2020

Thesis Chair: Cheng Zhu Ph.D.

© 2020 Mark F. Vail

Acknowledgments

I would like to express my gratitude and appreciation to Professor Cheng Zhu for his guidance and help throughout this research. This experience has set me up for success in my future professional career. I would also like to thank Dr. Chao-Sheng Tang from Nanjing University and Dr. Behrad Koohbar for their contributions to this research. I would like to thank my Thesis Committee for taking the time to review my thesis. I look forward to their feedback and the upcoming thesis defense.

I would also like to thank Zhuang Zhuo and Rui Liu for their contributions and input into the research. Our many discussions led to the overall success of this project. My engineering clinic students Luke Anderson, Mike Moroski, Nate Maute, and Jiwon Yang deserve thanks as well for their consistent effort and quality work throughout the entire project. These efforts allowed for efficient testing and obtained results throughout all studies.

I would also like to acknowledge the support from my parents Jeannie and Frank Vail, as well as, my girlfriend Joann Bodanza. Their constant support and belief in me gave me the opportunity to be successful in this program and reach my goal of achieving a Master's degree.

Abstract

Mark F. Vail

REMEDICATION OF DESSICATION CRACKING IN CLAYEY SOILS THROUGH
BIO-CEMENTATION AND BOTTOM ASH ADMIXTURE

2019-2020

Dr. Cheng Zhu Ph.D

Master of Science in Civil Engineering

Desiccation cracking considerably impairs the hydraulic and mechanical properties of clayey soils and is critical to the long-term performance of infrastructure foundations and earth structures. Classical crack remediation methods are associated with high labor and maintenance costs or the usage of environment-unfriendly chemicals. Recycling waste materials and developing bio-mediated techniques have emerged as green and sustainable soil stabilization solutions. The objective of this study is to investigate the feasibility of soil crack remediation through the usage of microbial-induced calcite precipitation (MICP) and bottom ash admixtures. We carry out monotonic drying and cyclic drying-wetting tests to characterize the effects of bottom ash and MICP on the desiccation cracking of clayey soils. The desiccation cracking patterns captured by a high-resolution camera are quantified using image processing and digital image correlation techniques. We also resort to scanning electron microscopy for microstructural characterizations. MICP treatment improves the soil strength due to the precipitation of calcite crystals on soil particle surface and inside inter-particle pores. Adding bottom ash into clay reduces the plasticity of the mixture, promotes the flocculation of clay particles by cation exchange, and also provides soluble calcium to enhance calcite precipitations. This study demonstrates the potential of using bottom ash and MICP for crack remediation and brings new insights into the design and assessment of sustainable infrastructures under climate changes.

Table of Contents

Abstract	iv
List of Figures	viii
List of Tables	x
Chapter 1: Introduction	1
Background	1
MICP	2
Bottom Ash Admixture	4
Image Analysis and Digital Image Correlation	5
Chapter 2: Research Objectives	8
Problem Statement	8
Research Hypothesis	8
Objectives of Study	8
Chapter 3: Desiccation Cracking Behavior of MICP-Treated Bentonite	11
Materials and Methodology	11
Soil	11
Bacteria and Cementation Solution	11
Sample Preparation	13
Testing Procedure	14
Image Processing and Quantitative Analysis	15
Results	17
Experimental Observation of Desiccation Cracks	17
Quantitative Analysis of Crack Patterns	19

Table of Contents (Continued)

Discussion.....	21
Crack Area Confidence Intervals.....	21
Effect of Solution Type on Water Evaporation	22
Effect of Solution Type on Crack Pattern.....	25
Significance and Limitation of Current Work	28
Summary of Findings.....	29
Chapter 4: Desiccation Cracking Behavior of Clayey Soils Treated with Bio-Cement and Bottom Ash Admixture	32
Methodology.....	32
Bottom Ash.....	32
Sample Preparation	33
Testing Procedure	34
Results.....	35
Experimental Observation of Desiccation Cracking Process	35
Quantitative Characterization of Crack Patterns.....	40
Discussion.....	42
Effect of Bottom Ash Admixture on Desiccation Cracking	42
Effect of Fluid Type on Desiccation Cracking	44
Effect of Treatment Cycle Number on Desiccation Cracking	46
Summary of Findings.....	48
Chapter 5: The Analysis of the Remediation of Desiccation Cracking of Sandy Clay with the Addition of Bottom Ash Admixture through Digital Image Correlation	50
Methodology.....	50

Table of Contents (Continued)

Test Setup..... 51

Sample Preparation 51

Imaging and Digital Correlation..... 52

Results..... 53

 Water Evaporating during Drying 53

 Volumetric Shrinkage during Drying 56

 Minor Principal Strain..... 60

Discussion..... 64

 Crack Area Confidence Intervals..... 64

 Effects of Bottom Ash 65

 Area of Interest Comparison..... 66

Summary of Findings..... 69

Chapter 6: Conclusions..... 71

References..... 75

List of Figures

Figure	Page
Figure 1. Experimental characterization of bacteria concentration and activity	13
Figure 2. Schematic view of the experimental setup of bentonite desiccation test	15
Figure 3. Procedure of digital image correlation	16
Figure 4. The spatiotemporal evolution of crack patterns in bentonite treated with different solutions	19
Figure 5. Segmented crack patterns of bentonite samples treated with various solutions at 48 hours.....	20
Figure 6. SEM image of partially cemented sample 75B25C	24
Figure 7. Probability distribution of crack area of four soil samples after 48 hours of drying	27
Figure 8. Probability distribution of crack width of four soil samples after 48 hours of drying	28
Figure 9. The evolution of geometrical parameters in soil samples subjected to wetting- drying cycles	41
Figure 10. SEM images of soil samples at the end of five cycles of treatments	44
Figure 11. The evolution of crack reduction rate with wetting-drying cycles.....	48
Figure 12. DIC area of interest	53
Figure 13. Moisture content over time.....	56
Figure 14. Contour maps showing the evolution of radial displacement at various time steps during drying of 0%BA sample	58
Figure 15. Contour maps showing the evolution of radial displacement at various time steps during drying of 20% BA sample	59
Figure 16. Contour maps showing the evolution of radial displacement at various time steps during drying of 40% BA sample	60

List of Figures (Continued)

Figure	Page
Figure 17. Contour maps showing the evolution of the second principal strain (ϵ_2) at various time steps during drying of 0% BA sample	62
Figure 18. Contour maps showing the evolution of the minor principal strain (ϵ_2) at various time steps during drying of 20% BA sample	63
Figure 19. Contour maps showing the evolution of the minor principal strain (ϵ_2) at various time steps during drying of 40% BA sample	64
Figure 20. Full A_1 , and reduced, A_2 , AOIs are shown for 0%BA sample	68
Figure 21. Variation of second principal strain, ϵ_2 , with respect to time for samples with 0%, 20%, and 40% BA	68

List of Tables

Table	Page
Table 1. Bentonite Clay Properties	11
Table 2. Quantitative analysis results obtained from the 48-hour crack patterns of six soil samples.....	21
Table 3. Desiccation time and water loss at the onset of cracking	23
Table 4. Fundamental properties of bottom ash.....	33
Table 5. Desiccation crack pattern in soils treated with water (group 1)	37
Table 6. Desiccation crack pattern in soils treated with MICP solutions (group 2)	39
Table 7. Characteristics of sandy clay gathered from Tech Park	51
Table 8. CIAS results	55
Table 9. Crack propagation over time.....	66

Chapter 1

Introduction

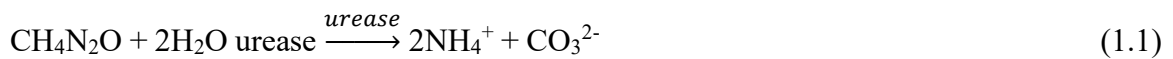
Background

Geological waste disposal is a globally preferred method for storing high-level radioactive waste. Municipal waste landfills remain the most common method of waste treatment worldwide. To ensure the long-term isolation of these geostorage systems, bentonite has been a favorable choice for buffering and backfilling because of its low permeability, high swelling, and high radionuclide retardation capabilities [1, 2]. Under drying or heated environment, soil moisture content decreases, and total volume shrinks. The resulting progressive formation of desiccation cracks imposes substantial negative impacts on the mechanical and hydraulic behaviors of clayey soils. These cracks undermine the mechanical integrity of the soil structure and cause a considerable weakening in soil strength [3, 4]. The extensive crack network formed by crack propagation and coalescence provides the dominant conductive pathways for fluid migration, resulting in an increase in the hydraulic conductivity of clayey soils by several orders of magnitude [5, 6], which is critical to the isolation functionality of the geostorage system [7]. The degradation of clayey soil properties due to the presence of desiccation cracks under climate changes is responsible for many geohazards, such as slope failure [8], embankment failure [9], and foundation and dam failure [10].

Research efforts have been dedicated to the development of soil improvement techniques for the remediation of desiccation cracking. Classical methods include mechanical and physical improvement by compaction control, surcharge loading, or soil

replacement, which are usually associated with high labor, high cost, and reduced long-term serviceability [11]. Chemical agents such as cement and lime have been used to reduce the shrinkage potential and suppress the crack development in soils [12, 13]. However, lime or cement additives did not completely suppress the soil desiccation cracking when the initial water content was high, and more importantly, might harm plant growth and cause irreversible environmental concerns [14]. The addition of fiber reinforcement has been adopted by a number of researchers in the past few decades (e.g., [15, 16]). Research results reveal that fiber inclusions significantly reduce the number of desiccation cracks in clayey soils. However, it remains challenging to minimize the agglomeration of fiber materials during mixing, especially at field scales[17]. These issues contribute to the necessity to develop a novel technology for soil crack remediation.

MICP. Microbial-induced calcite precipitation (MICP) has emerged in recent years as a potential solution for soil improvement. As a natural biological process, MICP is environment-friendly and low-maintenance based [18-20]. The fundamental mechanism of MICP can be characterized by the following equations, corresponding to two steps, respectively: (1) urea is hydrolyzed by microbial urease to form ammonium and carbonate ions; (2) the free calcium ions will react with the previously formed carbonate ions to generate calcite precipitations.



The addition of MICP has shown to biocement soil particles together. The calcite crystals formed from the MICP reaction engulf nearby soil particles together creating the

biocementation effect. This biocementation effect enhances the structural stability and decreases the permeability in sand mixed with MICP [18, 21]. MICP mixed with sand is able to form sand columns showing a homogenous solution between the MICP reaction and soil particles. These significant impacts allow for further investigation of MICP mixed with other soils

Typical geotechnical applications of MICP include the cementation of sands to enhance bearing capacity and liquefaction resistance[18] , soil erosion control [21], cracking healing in concrete and masonry [22], and remediation of radionuclide- and metal-contaminated soil [23]. So far, most research has focused on sand, whereas few studies have been reported on clayey soils. The main limiting factor lies in the small pore-throat size among clay soil particles that restrain the bacteria from passing freely [24]. Cheng and Shahin [25] used clayey sand with up to 20% clay content and assessed three MICP treatment methods including injection, premixing, and diffusion. Cardoso et al. [26] carried out oedometer and Brazilian splitting tests to characterize the biocementation effect on clayey sand and highlighted the importance of chemical effects originated from the clay fraction on soil behavior. Li et al. [27] blended fly ash at different concentrations into the MICP-treated expansive soil and showed that biocement and fly ash contributed jointly to the soil improvement. Guo et al. [28] demonstrated the potential benefit of MICP in remediating bentonite's desiccation cracking in the lab scale, and compared the cracking pattern based on visual observations. Most abovementioned studies only focus on the influences of MICP on the physical and mechanical properties of clayey soils, whereas there is still lack of knowledge in the quantitative analysis of the desiccation cracking behaviors of MICP-treated soils.

Bottom ash admixture. The usage of coal source for electricity generation leads to the production of an abundant quantity of coal ashes, including fly ash and bottom ash. Utilizing these waste materials significantly lowers the cost and contributes to the conservation of natural resources. A substantial amount of fly ash has been harnessed in the areas of geotechnical infrastructure, pavement, and roadway constructions [29]. However, due to the unique characteristics such as irregular shape, high porosity, low abrasion resistance, and potential to leach toxic trace elements, the utilization of bottom ash as an admixture is still restricted[30], with the primary use in the form of replacing soils and gravels for embankments, structural fill, road construction, concrete and other cement products. The potential impact of bottom ash admixtures on the volumetric shrinkage and desiccation cracking of clayey soils subjected to wetting-drying cycles remains poorly understood.

Combining bottom ash admixture and MICP solution into clay soils also is poorly understood. The combining effects will have unique impacts on the soil, and it is important to isolate the effects of each remediation technique. MICP solution is expected to add a biocementation effect onto the soil, as bottom ash is expected to reduce the plasticity of the soil through cation exchange and the agglomeration and flocculation of particles[31, 32]. Clay particles are surrounded by a diffuse hydrous double layer which is modified by the ion exchange of calcium. This alters the density of the electrical charge around the clay particles, which leads to the enhanced attraction and the formation of flocs, and eventually changes the soil texture [32, 33]. The negatively charged clay particles are engulfed by a diffuse hydrous layer that is altered due to the addition of positive ions such as calcium or other heavy metals. This alters the density of the soil particles and the electrical charge

surrounding each particle [33]. This leads to an enhanced attraction among particles and they begin to flocculate and agglomerate together. The particles gain more stability and bonding strength between the particles, and also limits the potential of soil expansion [31-33]. The exploration of these two effects simultaneously remediating desiccation cracking is yet to be fully quantified and analyzed

Image analysis and digital image correlation. Cracking behavior is difficult to predict and prevent. In general, crack branches join together and create crack networks, but initial cracking is difficult to determine [34]. Lab scale testing of desiccation cracking is exposed to the boundary and shape effects of the testing area. The understanding of the interaction between soil and testing surface is essential to characterize crack behavior. Most studies use petri dishes to study the desiccation cracking of soil. This implies the edges of the dish and bottom of the dish are fixed. These conditions affect the cracking behavior of the soil, and it is important to acknowledge these factors when studying crack formation. The relationship between the soil and boundaries of the petri dish is essential to understanding initial crack behavior in the lab scale. [35] The friction between the soil and petri dish edge determine the boundary impacts on cracking behavior. The petri dish typically represents a smooth surface, and the soil is a rougher surface. Higher surface friction between the soil and petri dish results in less shrinkage area [35]. A smooth soil surface will result in more shrinkage area of the soil sample due to the ability of the soil to expand easier. The interaction between the walls and soil are also very influential to the crack pattern. Cracks typically initiate from voids between the soils and walls of the boundary [36]. These cracks grow as water evaporates and eventually branch out onto the

soil surface. Image processing can be used to isolate these boundary conditions and explain other factors of the cracking phenomenon.

Using Digital Image Correlation (DIC), obtaining real-time radial displacement and minor principal strain is possible [37]. DIC uses the pixels of an original image and compares its location to the pixels of later images. Pixels are grouped together to form the studied area of interest (AOI). This original image represents zero displacement or strain, but as the drying process continues and cracking begins. The small groups of pixels begin to move or shift from their location in the original image. This change is captured using Digital Image Correlation and is represented as radial displacement or minor principle strain. This real time analysis allows for strain and displacement data without knowing the magnitude of the shrinkage forces being exerted on the soil sample [38]. DIC analysis allows for insight into soil behavior and crack formation during the drying process.

The following study aims to explore the potential of remediating desiccation cracking in clayey soils through the addition of MICP and bottom ash admixture. The structure of the defense is organized as follows. Chapter 2 discusses the hypothesis of this research and the overall objectives of the study, followed by Chapter 3 discussing the analysis of bentonite soil samples hand-mixed with MICP solution to determine and quantify the remediation effects of MICP. Chapter 4 includes the analysis of bentonite soil samples mixed with bottom ash undergoing cyclic treatments of MICP solution. This replicates the typical wetting-drying cycle behavior of field soil and examines the impacts of MICP once desiccation cracking has formed. Chapter 5 includes the analysis of the desiccation cracking of sandy clay soil samples mixed with bottom ash through Digital Image Correlation. This shows the remediation impacts of bottom ash, as well as, insight

into the crack propagation process. A summary of findings is included in chapter 6 describing the results of each experiment and exploring future expansion of this research.

Chapter 2

Research Objectives

Problem Statement

Desiccation cracking significantly decreases the structural integrity of clayey soils and is detrimental to the lifespan of many geotechnical structures. The prevention and repair of desiccation cracking would increase the serviceability of structures above clayey soil

Research Hypothesis

1. The additions of bio-cementation solution and bottom ash admixture can remediate desiccation cracking in clay soils.
2. The detailed analysis using image processing tools can lead to a better understanding of crack network propagation and the behavior of soil under wetting and drying conditions.

Objectives of Study

The primary focus of this thesis is the remediation of desiccation cracking in clayey soil. The desiccation cracking is analyzed through the study of crack formations over time using image processing and other tools to quantify and compare crack segments. The effectiveness of crack remediation techniques can be observed visually and quantitatively throughout this study. The paragraphs below describe the research objectives of the following chapters.

Chapter 3 discusses the addition of an environmentally friendly and cost-effective remediation technique of desiccation cracking in clay soils known as MICP. MICP has

been rarely studied in clay soils due to the small pore sizes that may limit the effectiveness of the treatment. This study intends to show the feasibility of using MICP as a remediation method through hand mixing in bentonite clay. The reduction of desiccation crack area would show MICP has an impact on the soil structure and creates a stronger bonding strength between particles. Using a crack image analysis software, different crack parameters can be measured and used to understand better desiccation cracking formation and remediation. This chapter also compares the desiccation cracking of different ratios of MICP solutions and the impact each ingredient has on individual bentonite clay samples.

This study aims to characterize the effect of MICP on the remediation of desiccation cracking in bentonite soils. To overcome the difficulty of fluid migration in low-permeability bentonite, we mixed bentonite with different percentages of bacteria and cementation solutions and prepared six types of soil samples. Other stabilizing agents are not considered in this study to eliminate potential influences on the results. Desiccation drying tests were carried out, with cracking morphology captured by a high-resolution camera and quantified through image processing.

Chapter 4 discusses the lab-scale application of the MICP injection technique, and the effect the addition of bottom ash admixture has on desiccation cracking. Bentonite samples are subjected to MICP treatments and Water Treatments to replicate wetting drying cycles that occur naturally in the field. This comparison shows the significant impacts of MICP injection and its inherent healing capabilities through cyclic treatments. Bentonite is mixed with bottom ash to determine the effect of the admixture on desiccation cracking. This chapter focuses on the combination of bottom ash and MICP injection treatments to remediate desiccation cracking.

The understanding of wetting and drying cycles is essential to the understanding of desiccation cracking as this is the typical lifespan of clayey soils exposed to the atmosphere. This experiment focuses on the comparison between water injected samples (Control) and MICP injected samples (Test). Direct insight into the remediation effects of bottom ash and MICP injection treatments is shown in chapter 4.

Chapter 5 analyzes the desiccation cracking in sandy clay soil. This would be considered a more field applicable soil. This analysis is conducted using Crack Image Analysis Software (CIAS) and Digital Image Correlation. Bottom ash admixture is again added to the soil to measure its impact further. The real-time crack analysis shows insight into future crack patterns and allows for detailed comparisons of minor principal strain and radial displacement. This comparison highlights the impacts of bottom ash in remediating desiccation cracking and the impact it has on crack formation.

Chapter 3

Desiccation Cracking Behavior of MICP-Treated Bentonite

Materials and Methodology

Soil. This study uses the calcium bentonite clay provided by Bulk Apothecary Inc. for testing. We performed sieve analysis and hydrometer analysis to get grain size distributions, and Atterberg limit tests to determine the soil plasticity. Table 1 summarizes the physical properties of the original soil. According to the Unified Soil Classification System (USCS), this soil is classified as clay of high plasticity (CH). According to the analysis result provided by Bulk Apothecary Inc., its clay fraction is dominated by montmorillonite, and the soluble calcium amount is 21.2 meq.

Table 1

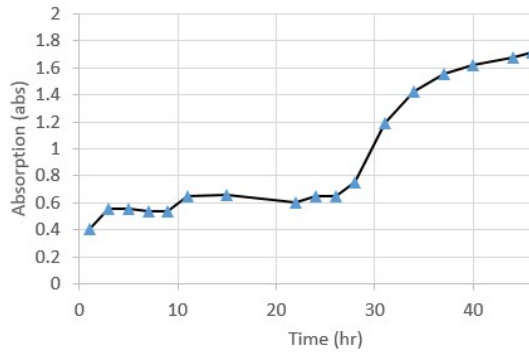
Bentonite Clay Properties

Properties	Value
Specific gravity	2.6
<i>Consistency limit</i>	
Liquid limit (%)	276
Plastic limit (%)	37
Plasticity index (%)	239
pH	8.5
USCS classification	CH
Clay ($< 2\mu m$)	46%

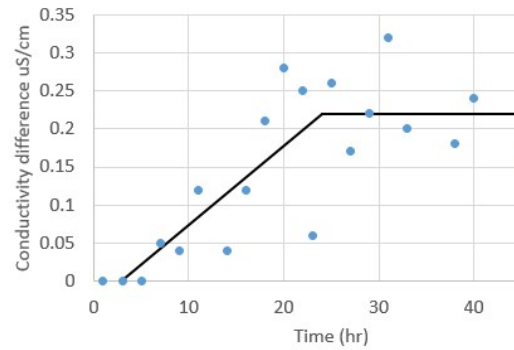
Bacteria and cementation solution. In this study, we used a urease-active strain *Sporosarcina pasteurii* (ATCC 11859) for the MICP treatment because of its well-defined urease-synthesis behavior and strong biological activity under alkaline environment [39].

To initialize the growth of bacterial colonies, we rehydrated pure bacterium strain in the solid ammonium yeast extract (NH₄-YE) medium for 24 hours followed by low-temperature storage in Petri dishes at 4°C. High bacterial concentration could be reached through the incubation of bacteria in the liquid bacterial growth medium. We prepared the growth medium by mixing 20 g/L yeast extract, 10 g/L ammonium sulfate, 15.73 g/L Tris base. We sterilized each ingredient of the medium in an autoclave at 121°C for 20 minutes before mixing. After inoculation of the bacteria from the solid NH₄-YE medium into the liquid bacterial growth media, we started the incubation process by shaking the flask inside an incubator at a rotation speed of 200 rpm under a constant temperature of 30°C. The optical density (OD₆₀₀) value was adopted as an indicator of the bacteria concentration, measured using an ultraviolet spectrophotometer at 600 nm wavelength. Continual measurements indicated that OD₆₀₀ increased with time and reached an ultimate range of 1.724 absorbance after 48 hours (Figure 1a). To further assess the bacteria activity based on the concentration of ammonium produced from urea, we resorted to the measurement of the electrical conductivity of the bacteria solution [40]. As the bacteria became more active and helped produce more ammonium, the electrical resistivity of bacteria solution increased, and gradually stabilized after approximately 24 hours (Figure 1b). Therefore, to ensure maximum activity, the bacteria used in this study were incubated for 24-48 hours.

To prepare the cementation solution, we followed previous literatures [41, 42] and selected 0.5 M/L as the solution concentration in this study. As a result, every liter of cementation solution comprised 0.5 mole of urea, 0.5 mole of CaCl₂, and 3 g of nutrient broth.



(a)



(b)

Figure 1. Experimental characterization of bacteria concentration and activity: (a) absorption (OD_{600}) measured from spectrophotometer; (b) increase in electrical conductivity measured from the electric conductometer.

Sample preparation. The soil was air-dried, crushed and passed through the #200 sieve. To investigate the influences of pore fluids on soil cracking behavior, different specimens with varying fluid compositions were prepared. Each bentonite mixture has a moisture content of 100%, which corresponds to the following six types of pore fluids: (a) 100% pure deionized water (considered as control mixture, denoted as sample W); (b) 100% bacteria solution (denoted as sample B); (c) 100% cementation solution (denoted as sample C); (d) 25% bacteria solution and 75% cementation solution (denoted as sample 25B75C); (e) 50% bacteria solution and 50% cementation solution (denoted as sample 50B50C); and (f) 75% bacteria solution and 25% cementation solution (denoted as sample 75B25C). The mixture of bacteria and cementations solutions is denoted as solution BC in this manuscript. MICP-treated samples refer to sample types (d), (e), and (f). As the initial water content was less than LL, the desiccation cracking of bentonite started from an unsaturated state, which aims to avoid excessive cracking. 100% fluids were added into the

dry bentonite for mixing. Each mixing process continued for 10 minutes until the mixture reached a homogeneous state. For each mixture type, three parallel samples were made to validate the experimental repeatability. Moist soils were molded into the 50-mm diameter Petri dishes (inner depth = 6.35 mm) and fill the volume completely.

Testing procedure. All soil samples underwent the same desiccation process, with each mixture placed in a Petri dish and exposed to relatively stable room conditions at a temperature of 30 ± 1 °C and a relative humidity of $50\% \pm 5\%$ for drying. Figure 2 demonstrates the schematic view of the experimental setup. The Petri dish containing the bentonite sample was placed on a scale, to monitor the temporal change of soil weight continuously. Under LED light conditions, a high-resolution digital camera mounted on top captured the evolving desiccation crack patterns in bentonite samples for subsequent image processing and quantitative analyses. To further characterize soil microstructural changes, we made observations through the scanning electron microscopy (SEM) on the completely dried samples.

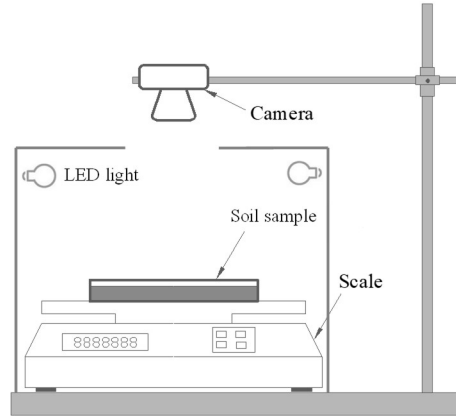


Figure 2. Schematic view of the experimental setup for bentonite desiccation test

Image processing and quantitative analysis. To quantitatively compare the effects of various fluids on the soil desiccation process, an image processing software “Crack Image Analysis System” (CIAS) developed previously [43] was used here. As shown in Figure 3, the image processing comprised three major steps. First, the original color image showing crack patterns (Figure 3a) was converted into a grey-level image (Figure 3b). Then, by applying the binarization operation using a simple gray threshold, we were able to distinguish cracks from soil clods through their sufficiently high contrasts (Figure 3c). At last, after the removal of noises in the binary image through a filter operation (Figure 3d), CIAS automatically outlined the skeleton of crack networks (Figure 3e). The final segmented crack network (Figure 3f) was used to determine the following geometrical parameters: (1) Surface crack ratio R_{sc} , referring to the ratio between the crack area and the total surface area of the soil sample; (2) Average width of cracks W_{avg} , determined by calculating the shortest distance from a randomly chosen point on one boundary to the crack’s opposite boundary; (3) Total length of cracks L_T , determined by

calculating the trace length of the medial axis of the crack segment, reflected as the skeleton in Figure 3f; (4) crack segment number n_c , indicating the total number of cracks after segmentation, and (5) average crack length L_{avg} , calculated as the ratio between total crack length and crack segment number (i.e., $L_{avg} = L_T/n_c$). More details on the crack pattern descriptors are available in [43].

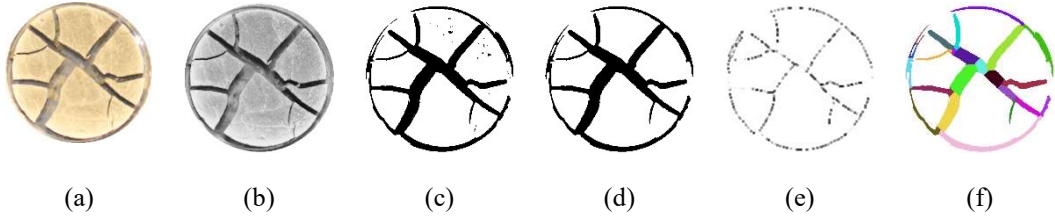


Figure 3. Procedure of digital image processing: (a) original image, (b) grey image, (c) binary image, (d) clear noise and smoothing, (e) skeleton of the crack network, and (f) crack segmentation.

To further analyze the distribution features of the crack pattern, we calculated the density function of two crack geometry descriptors, including crack area A and crack width W . Take crack width for instance, the density function of crack width $f(W)$ is a density of crack width corresponds to value W and defined as [43]:

$$f(W) = \frac{\Delta n_W}{n_c \cdot \Delta W} \quad (3.1)$$

in which n_c is the total number of crack segments, Δn_W is the number of crack segments whose width ranges between ΔW . The fraction of the crack width in the range of W and

$W + dW$ is given by $f(W)dW$. If the crack width in a given crack pattern covers from length a to b , we have

$$\int_a^b f(W)dW = \int_0^{n_c} \frac{dn}{n_c} = \frac{1}{n_c} \int_0^{n_c} dn = 1 \quad (3.2)$$

This means that the number of crack segments whose value fall into the interval $[a, b]$ equals the total number of crack segments, n_c . We adopted the concept of the most probably value (MPV) of crack width, corresponding the width when the maximum value of $f(W)$ is achieved [39]. Therefore, the probability of crack width near MPV is maximal during cracking. Probability distribution and MPV values are determined for crack area in a similar way.

Results

Experimental observation of desiccation cracks. Figure 4 presents desiccation cracks captured at regular time intervals (12, 24, 36, and 48 hours) for all six types of samples. For each mixing type, three parallel samples give comparable crack pattern results, verified by the subsequent image analysis. All samples experienced extensive cracking, with soil body split into separate clods by crack segments. During the drying process, we observed the process of crack initiation, propagation, coalescence, and intersection, leading to the formation of a complicated crack network throughout the soil sample. Cracks initiate from the weaker regions such as natural pores in the soil [44], propagate under the driving force of capillary suction, and bifurcate from primary into secondary crack branches. Experimental observations indicate that crack pattern changed most significantly during the rapid decrease of moisture content within 12-36 hours. After 48 hours, crack pattern remains unchanged while the water content stopped decreasing.

The post-evolutions of crack patterns are mostly the broadening of crack width without generating any new crack branches.

Due to the effect of mixing fluids, six types of samples exhibit different cracking morphologies. Comparing these samples, after 12 hours, considerable desiccation cracks were observed in samples W, B and C, whereas MICP-treated samples remain intact (row “12-hr” in Figure 4). This highlights the effect of MICP in delaying soil cracking and enhancing the soil strength. At 24 hours, primary cracks, secondary cracks, and the separation between soil and Petri-dish boundary become apparent. Secondary cracks initiate from a primary crack or the circumferential boundary of the specimen (row “24-hr” in Figure 4). The widths of primary cracks in samples W, B and C are much larger than those of MICP-treated samples. As water content decreases, the growth of new secondary cracks continues, especially in MICP-treated samples. In all samples, crack width increases significantly. As the soil layer thickness is 0.635 cm, at the end of 36 hours, most primary cracks have propagated to the bottom of the Petri dishes, as reflected by the visible dish bottom (row “36-hr” in Figure 4). In the following 12 hours, crack width continues to increase whereas the crack pattern stayed almost unchanged (row “48-hr” in Figure 4). It is interesting to note that, in comparison to sample W, bentonite samples treated with MICP exhibit a certain extent of color change on the soil surface from yellow to white (row 48-hour). This color change implies the precipitation of calcium carbonate (CaCO_3) film on soil surface resulting from the bio-cementation process. Although visual observations provide a qualitative view of the evolving crack pattern, the changes in crack width and crack length are difficult to quantify, requiring further image analysis of the crack pattern.











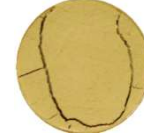










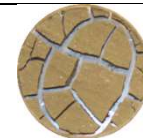


T (hrs)	Sample W	Sample B	Sample C	Sample 25B75C	Sample 50B50C	Sample 75B25C
12						
24						
36						
48						

Figure 4. The spatiotemporal evolution of crack pattern in bentonite treated with different solutions (Time = 12, 24, 36, and 48 hours).

Quantitative analysis of crack patterns. To quantify the evolving characteristics of crack patterns, we performed image analysis on all final crack patterns at the end of 48 hours. Crack segments generated from the image processing of the final crack pattern at 48 hours are shown in Figure 5, with different colors representing different crack segments. The final crack pattern consists of both shrinkage cracks and the circumferential edge-soil separations. Based on these crack segments, we determined five geometrical parameters as defined in section 2.5, including surface crack ratio, the average width of cracks, and total length of cracks, crack segment number, and average crack length.

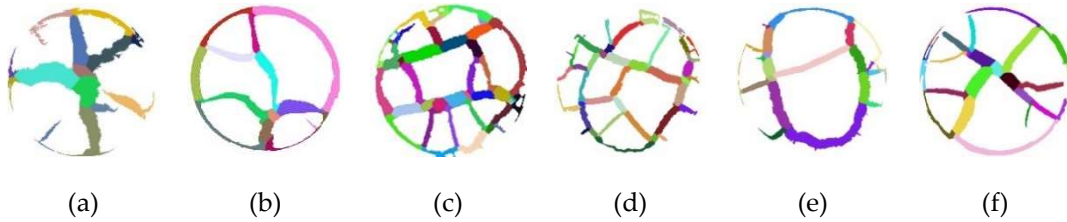


Figure 5. Segmented crack patterns of bentonite samples treated with various solutions at 48 hours: (a) sample W, (b) sample B, (c) sample C, (d) sample 25B75C, (e) sample 50B50C, and (f) sample 75B25C.

As shown in Table 2, mixing MICP solution with bentonite effectively mitigates soil desiccation cracking and reduces the surface crack ratio by up to 23%, from the maximum value of 29.2% (sample W) to the minimum value of 22.6% (sample 50B50C). Sample 50B50C gives slightly lower surface crack ratio than other two MICP-treated samples, highlighting the importance of solution fraction ratio in optimizing the bio-cementation effect. Over-supply of bacteria or cementation solutions does not necessarily increase the amount of calcite precipitations. Samples W and C give comparable surface crack ratios, whereas sample B gives a much lower surface crack ratio.

In terms of average crack width, sample W gives the largest value, 65% higher than that of sample 25B75C. Except for samples W and sample C, other samples share comparable smaller average crack width at 0.17-0.18 cm. Due to the much larger crack width, total crack length of sample W is the smallest. Among MICP-treated samples, sample 50B50C gives the smallest total crack length.

The correlation between surface crack ratio and crack number is not clear, which requires further investigations in the future. In this study, sample C presents the highest number of cracks, whereas sample W gives the lowest. Due to the presence of high crack segment number, samples C and 25B75C give the lower average crack length. On the contrary, sample W with the minimum crack segment number has the largest average crack length of 1.46 cm.

Table 2

Quantitative analysis results obtained from the 48-hour crack patterns of six soil samples.

Crack Parameters	Sample W	Sample B	Sample C	Sample 25B75C	Sample 50B50C	Sample 75B25C
Surface crack ratio (%)	29.2	24	29	25.7	22.6	23.5
Average crack width (cm)	0.28	0.18	0.20	0.17	0.18	0.18
Total crack length (cm)	23.4	28.8	36.2	34.2	29.0	31.7
Crack segment number (-)	16	28	44	41	24	25
Average crack length (cm)	1.46	1.02	0.82	0.83	1.21	1.27

Discussion

Crack area confidence intervals. 95% confidence intervals of each sample show major differences when comparing crack areas. Sample W has a difference of 1.94%, Sample B possesses a difference of 1.39%, Sample C possesses a difference of 2.08%, Sample 5B75C possesses a difference of 1.11 percent, Sample 50B50C possesses a

difference of 1.38%, and Sample 75B25C has a difference of 1.25% Crack areas among MICP treated samples and Sample B show a similar 95 % confidence interval range, indicating minimal significant differences between ranges of crack areas between these sample. However, Sample 50B50C still maintains the lowest range of crack area and shows the impact of optimizing the MICP solution. Sample C and W also obtain similar confidence interval due to similar crack patterns and areas. Cementation solution and water have similar effects on the soil body resulting in similar crack areas with no significant difference between the samples in terms of crack area.

Effect of solution type on water evaporation. Desiccation cracking process occurs after a certain extent of water loss. Understanding the water evaporation process and identify the critical water content is key to the study of the cracking process. In this study, critical water content refers to the water content when first desiccation crack initiates. We found that, in all samples, the circumferential soil-dish separation occurred later than desiccation cracks. Comparing the desiccation time at the onset of cracking, the formation of cracks was first observed after 2.5 hours in sample W, followed by 4.5-5 hours in samples B and C, and then > 16 hours in samples treated with MICP (Table 3). This further validates the effects of MICP in strengthening the soil body and lowering the cracking potential. The critical water content at crack initiation could be obtained based on the change of the soil total weight. When cracks initiated, sample W still has a high-water content at 93.5%, in comparison to the initial water content of 100%. Other samples exhibit lower water content levels at the onset of desiccation cracking, thus correspond to more water loss. The general trend is that when cracks first appeared, larger total weight change was recorded in MICP-treated samples, implying a larger amount of water evaporation than

other samples. Under drying, water evaporation results in matrix suction and soil volume shrinkage, forming a tensile stress field. Cracks initiate when the tensile stress exceeds the tensile strength of the soil. Samples treated with MICP gain higher strengths as a result of the biocementation effect, which thus requires a larger driving force associated with more water evaporation to satisfy the cracking criterion.

Table 3

Desiccation time and water loss at the onset of cracking

Sample Type	W	B	C	25B75C	50B50C	75B25C
Crack initiation time (hr)	2.5	5	4.5	16.5	16	17
Critical water content	93.5%	81%	85%	72%	77.3%	66.6%

In general, the evaporation process can be divided into three stages [45]: (1) constant rate stage; (2) falling rate stage; and (3) residual rate stage. At the constant rate stage, the soil remains saturated and the evaporation rate is dominated by ambient factors. Desiccation cracks start to develop in the constant rate stage when the soil remains saturated. After drying, when air starts to replace water in the pores and soil changes from saturated to unsaturated state, the evaporation process transits to the falling rate stage. Therefore, the transition point of the evaporation curve corresponds to the air-entry state of soil. Given the soil tested here had a water content of 100%, less than the liquid limit, only falling rate and residual rate stages should be observed. However, in this study, these two phases were not observed in MICP-treated samples. This can be attributed to two factors, the hydrolysis of urea and the bio-mediated soil reinforcement. According to Eq.

(3.11), water is involved during the hydrolysis reaction, which considerably lowers the water amount that is available for evaporation under drying. Therefore, at the end of desiccation test, the percentage of water loss, defined as the ratio between water loss and the original water amount, is 50%, 60%, and 58% for samples 25B75C, 50B50C, and 75B25C, respectively. On the other hand, the precipitated calcite in Eq. (3.2) acting as a bonding agent to bentonite clay particles delays and reduces the soil cracking process. The presence of less cracks decreases the soil surface area that is in contact with atmosphere, contributing to the slow down and reduction of the moisture loss. SEM observations validate this phenomenon. As shown in Figure 6, in sample 75B25C, white region corresponds to the area where full biocementation occurred, whereas grey regions represent less-cemented areas. Micro-pores of different sizes mostly exist in the less-cemented areas. Such pores could be caused by the evaporation of water and the continued volumetric shrinkage of soil body. SEM observations also highlight the microstructural heterogeneity under the coupled effects of biocementation and water evaporation.

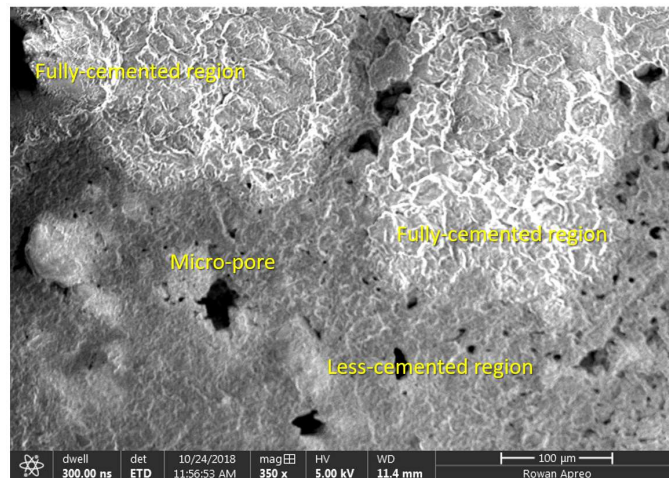


Figure 6. SEM image of the partially cemented sample 75B25C.

Comparing three MICP-treated samples, higher amount of water loss was observed in samples 50B50C and 75B25C, implying the influences of bacteria and cementation amount on the biocementation effect. Although the calcium bentonite used in this study provides sufficient soluble calcium ions, the hydrolysis reaction is governed by the presence of both urea and the urease-producing bacteria. Zhao et al. [46] showed that, the calcite content and the sandy soil strength increased with increasing bacteria, whereas more cementation media has limited effects in enhancing MICP results. Consistent findings were obtained in our study. As reflected through water loss, sample 50B50C reached 60%, higher than both samples 25B75C and 75B25C, indicating a better biocementation effect. Urea is provided by the cementation solution, and urease activity is determined by the bacteria solution. Therefore, more bacteria or more cementation solution in the mixture may not necessarily enhance the MICP process.

Effect of solution type on crack pattern. To study the effect of soil type on desiccation crack pattern, we carried out the quantitative analysis of crack geometrical parameters. The probability density functions of crack parameters including crack area and crack width, as described in section 2.5, are determined to compare the solution effect on final crack pattern.

The probability distributions of crack areas can be approximated by the power law distribution, with much higher probability value obtained for smaller cracks and very small probability value for larger cracks (Figure 7). The area of most cracks in all samples is below 0.2 cm^2 , whereas more than 40% of the cracks in sample W have an area larger than 0.3 cm^2 . Although the MICP process could not be initiated in samples B and C, large cracks are not visible. The surface crack ratios of samples W, B and C (Table 2) are not able to

reveal the distribution features. Although samples W and C share similar value of surface crack ratio, their probability distributions vary significantly. In general, when cementation solution is added to the clayey soil, Ca^{2+} ions replace monovalent, metallic ions surrounding the clay particles. Clay particles are surrounded by a diffuse hydrous double layer which is modified by the ion exchange of calcium. This alters the density of the electrical charge around the clay particles, which leads to the enhanced attraction and the formation of flocs, and eventually changes the soil texture [32, 33]. However, in our study, cementation solution has little effects on the cracking of sample C, which is mostly because the bentonite soil is rich in Calcium and has formed a relatively stable soil structure. If other type of clayey soil such as sodium bentonite was used, the addition of cementation solution will show a much stronger cementation effect [31]. In sample B mixed with bacteria solution, numerous microbes fill up the inter-particle pores and adhere to the surface of soil particles, which may induce the formation of biofilms on soil particles and affect the physical properties of soil [47].

Among three MICP-treated samples, sample 50B50C has the highest probability distribution of small cracks with area less than 0.1 cm^2 (Figure 7), validating the best cementation effect in this sample. Although sample 25B75C shows a larger surface crack ratio than sample 75B25C, majority of its cracks are limited to $0\text{-}0.2 \text{ cm}^2$. Comparatively, sample 75B25C has less small cracks and has a broader range of crack area. The most probable values (MPV) of samples B, 25B75C, 50B50C, and 75B25C are within the range of $0\text{-}0.1 \text{ cm}^2$, while the MPV values of samples W and C are around $0.1\text{-}0.2 \text{ cm}^2$.

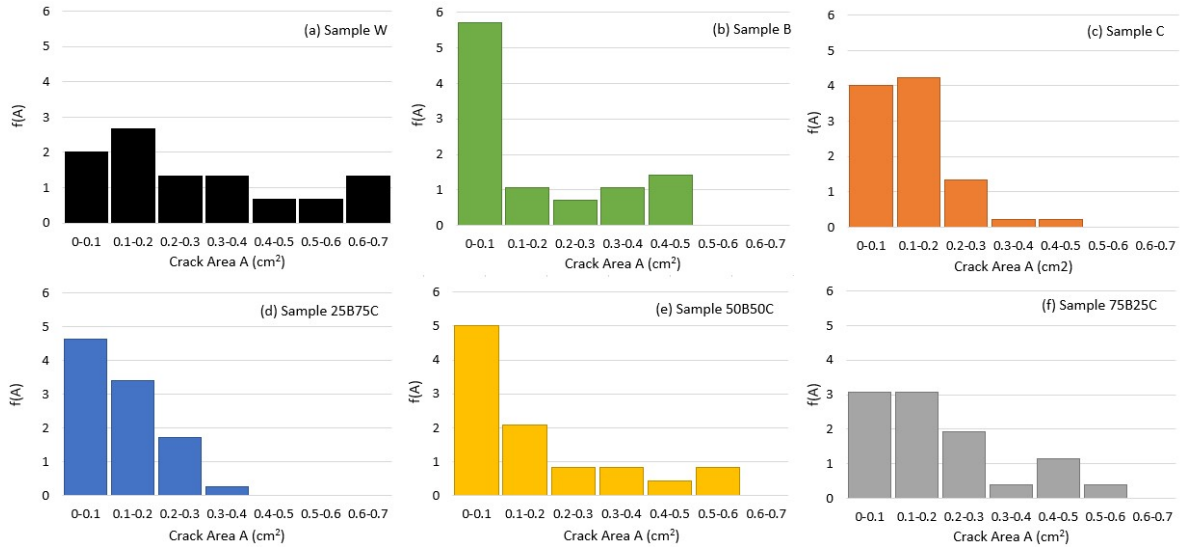


Figure 7. Probability distribution of crack area of four soil samples after 48 hours of drying.

Figure 8 shows the probability distribution plots of crack width, which is different from that of crack area. This is because larger cracks may have small widths but large lengths. While majority of the cracks in the MICP-treated samples belong to narrow cracks with width less than 0.2 cm, 50% of the cracks in sample W are larger than 0.25 cm wide. Sample W has a much broader range of crack width varying from 0 to 0.7 cm than all other samples. Comparing all samples, cracks in sample B are more uniform, as demonstrated by the high probability value for both crack area (0-0.1 cm²) and crack width (0.1-0.2 cm). In this study, MPV for crack width is 0.1-0.2 cm for samples B, C, 25B75C and 50B50C, and 0-0.1 cm for samples W and 75B25C. These probability distribution plots provide a better quantitative overview of the crack pattern.

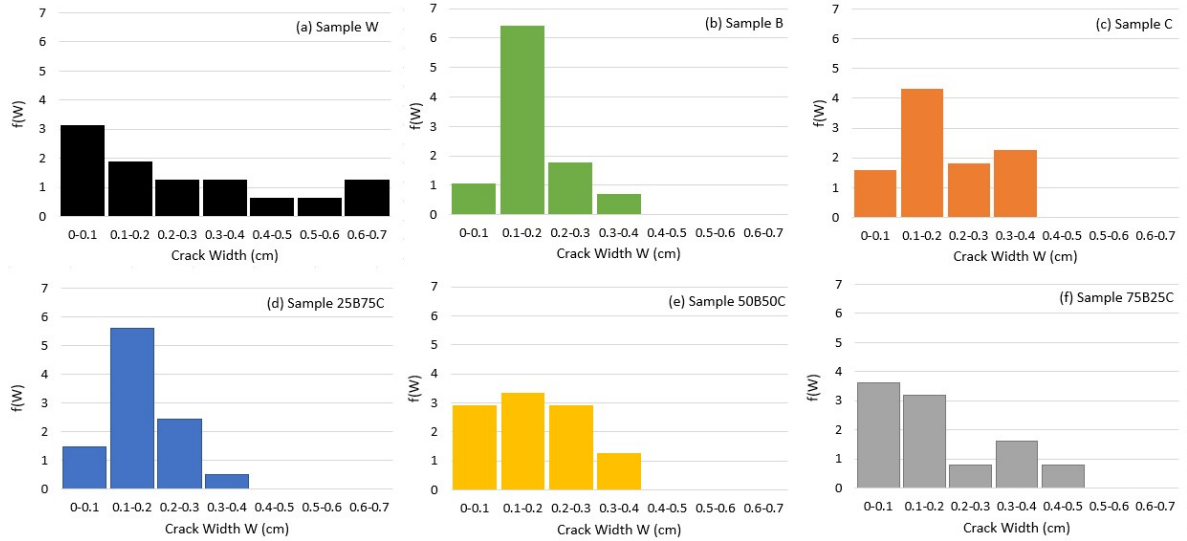


Figure 8. Probability distribution of crack width of four soil samples after 48 hours of drying.

Significance and Limitation of Current Work

Our research indicates that mixing MICP solutions with bentonite soils restrains the shrinkage cracking and reduces the crack geometric parameters, particularly surface crack ratio and average crack width. As introduced earlier, the variation of the crack geometry governs the hydraulic and mechanical properties of soil. In comparison to the control sample, MICP-treated bentonite is expected to possess an improved hydraulic conductivity and mechanical strength due to the bonding effect of CaCO_3 produced in the MICP process. The improved structural integrity of MICP-treated bentonite is of great importance to the performance of geological storage systems.

The MICP treatment presents several advantages over existing soil improvement techniques. Our study indicates that MICP treatment can delay the crack initiation and suppress the soil desiccation cracking significantly at high initial water content, because of

the remarkable water stability of calcite mineral produced in the MICP process. For clayey soils with calcium contents, the MICP treatment effect can be optimized given appropriate amount of bacteria and cementation solutions. As a natural biological process, the MICP is a more environment-friendly and energy efficiently solution for soil desiccation cracking remediation. Moreover, the residual urea in soil during the MICP process can provide nutrients for plant growth.

This study has demonstrated the feasibility of using MICP to remediate desiccation cracking in small bentonite soil samples at lab scale. The mixing process remains to be tested for field implementations. The bio-grouting and injection methods will be extremely challenging for bentonite due to its small pores and low permeability. Alternative approaches such as surface spraying of MICP solution may be a better solution. Due to the scale and boundary effects, lab results still show large deviations with field measurements. For instance, compared to the field tests reported by Li and Zhang [48], the crack length is shorter and crack density is higher in the small soil sample of the current study. In addition, the crack distribution is more inhomogeneous in field tests, as the soil often contains coarse particles and structures, and has more complicated interactions with the varying atmosphere in field. To investigate the potential application of MICP for soil crack remediation in field, more in-situ tests will be needed. Furthermore, the influence of MICP on the crack depth is not considered and will be studied in the future work.

Summary of Findings

The formation of desiccation cracks in bentonite soils is detrimental to the long-term performance of engineered clay barriers in geological storage facilities. In this study, we investigated the potential of the MICP treatment in the remediation of desiccation

cracks for bentonite. Laboratory desiccation tests were conducted on bentonite samples mixed with deionized water, bacteria solution, cementation solution, or different percentages of bacteria and cementation solutions. Relying on imaging tools including camera and SEM, we carried out qualitative and quantitative analyses on soil cracking behaviors and reached the following conclusions:

(1) MICP significantly delays the initiation of desiccation cracks in bentonite soils. The formation of cracks was first observed in sample treated with water after 2.5 hours of drying, followed by 4.5-5 hours in samples treated with bacteria or cementation solutions, and then more than 16 hours in samples treated with MICP.

(2) MICP-treated soil samples show less desiccation cracks, as reflected by the surface crack ratio and average crack width. Under the MICP process, the calcite crystal precipitations contributes primarily to the improved mechanical integrity of soil sample as well as desiccation cracking resistance. The sample treated with bacteria solution also gives less cracks as a result of the formation of biofilm around clay particles due to the presence of microbes. For calcium bentonite, cementation solution containing calcium chloride has negligible impacts on the remediation of soil cracking.

(3) The water evaporation in MICP-treated samples is governed by two factors including the hydrolysis of urea and the bio-mediated soil reinforcement. More water loss is needed in MICP-treated samples to generate larger suction stresses as the crack driving force. More bacteria or more cementation solution in the mixture may not necessarily reduce the water evaporation.

(4) The probability distributions of crack areas can be approximated by the power law distribution. The MPV of crack areas for samples B, 25B75C, 50B50C, and 75B25C

are within the range of 0-0.1 cm², while that of samples W and C are around 0.1-0.2 cm². Most cracks in the MICP-treated samples are narrow with width less than 0.2 cm, whereas 50% of the cracks in sample W are larger than 0.25 cm wide. MPV for crack width is 0.1-0.2 cm for samples B, C, 25B75C and 50B50C, and 0-0.1 cm for samples W and 75B25C.

This study validates the applicability of MICP treatment in reinforcing clayey soils for drying conditions. Bonding crystals produced from MICP enhances the soil strength and lowers the potential of desiccation cracking in clayey soils. Future study will focus on the application of multiple MICP treatments in clayey soils. The bio-stabilization of clayey soils explored in this study brings new insights into the remediation of soil erosion and cracking for various climate changes, which is key to the design and performance of sustainable geotechnical infrastructures.

Chapter 4

Desiccation Cracking Behavior of Clayey Soils Treated with Bio-Cement and Bottom Ash Admixture

Methodology

This study aims to explore the potential of remediating desiccation cracking in clayey soils through the addition of bottom ash mixtures and the MICP-based biocementation technique. To test the feasibility of this method in reinforcing extremely swelling soils, bentonite is chosen as the experimental clay material. Instead of pre-mixing, we adopted the surface spraying method to add bacteria and cementation solutions into the soil. The structure of the paper is organized as follows: Methodology explains materials used, sample preparation, and test setup. Results section presents experimental observations of desiccation crack patterns and quantitative image analysis results. Discussion section emphasizes the influences of bottom ash, fluid type, and wetting-drying cycle on soil cracking behaviors. The major findings obtained from this study are summarized in the conclusions section.

Bottom ash. The fundamental properties of bottom ashes provided by Charah Solutions, Inc. are summarized in Table 4. The low unit weight can be attributed to two factors: (1) chemical compositions, and (2) presence of particles with porous or vesicular textures. The chemical composition indicates that bottom ash contains a significant amount of CaO, which may facilitate the precipitation of calcite during the reaction. In addition, several types of heavy metals exist, which is the main cause of the potential environmental

hazard of bottom ash. Researchers have explored the possibility of bioremediation of heavy metal-contaminated soils through MICP [49, 50].

Table 4

Fundamental properties of bottom ash

Properties	Value
Unit weight	15.31 kN/m ³
Percent finer (pass #100)	<17%
<i>Chemical Composition</i>	<i>Percentage by weight</i>
CaO	17.28
SiO ₂	40.706
Al ₂ O ₃	14.997
Fe ₂ O ₃	5.706
MgO	7.214
SO ₃	0.527
Mn ₂ O ₃	0.019
TiO ₂	1.596
P ₂ O ₅	0.2714
ZnO	0.0083

Sample preparation. Bentonite clay was crushed, air dried, and sieved through the #200 sieve. As an experimental investigation, relatively fine bottom ash particles that

passed #30 and retained above #60 sieves were selected in this study, which ensured the homogeneous mixing with smaller clay particles and minimized the formation of local defects. We prepared two groups of samples, group 1 for pure water treatments, and group 2 for MICP treatments. Each group contains three samples, with different mixing ratios by weight: (a) 100% bentonite (sample A); (b) 80% bentonite and 20% bottom ash (sample B); and (c) 60% bentonite and 40% bottom ash (sample C). One hundred percent (100%) water by weight were added into dry samples and mixed continuously until reaching a homogeneous state, which is denoted as treatment 0 in this study. To validate the experimental repeatability, we made three parallel samples for each mixing ratio under each treatment type. Moist soils were molded into the 50-mm diameter by 6.35-mm depth Petri dishes, with surface leveled appropriately.

Testing procedure. The experiments were performed in a relatively stable environment (30 ± 1 °C in temperature, $50 \pm 5\%$ in relative humidity). During the test, in addition to the preliminary wetting-drying cycle (denoted as treatment 0), all samples underwent five subsequent treatment cycles (denoted as treatments 1-5), with each treatment made through the surface spraying of the same amount of fluids (i.e., water or MICP solutions). We initiated the new treatment cycle only after the soil sample became completely dried and its mass stayed constant. Samples were placed underneath a high-resolution camera in an enclosed area with isolated light sources. After each wetting-drying treatment cycle, soil crack patterns were captured by a high-resolution digital camera mounted on top for further image-based quantitative analyses [43]. Microstructural characterization of dried samples was carried out using Scanning Electron Microscope (SEM) (at the end of five treatment cycles)

Based on the final crack pattern obtained from image processing, we determined three geometrical parameters [43]: (1) Surface crack ratio R_{sc} , calculated as the ratio between the crack area and the total surface area of the soil sample; (2) Average crack width W_{avg} , determined by the shortest distance from a randomly chosen point on one boundary to the crack's opposite boundary; and (3) Total crack length L_T , calculated as the trace length of the medial axis of crack segment, reflected as the skeleton in Figure 3e.

Results



















Experimental observation of desiccation cracking process. Table 5 and Table 6 present the typical desiccation crack patterns captured at the end of each cycle for samples treated with water and MICP solutions, respectively. Due to the presence of bottom ash, samples exhibit a different extent of cracking at the beginning (row “Treatment 0”). Cracks initiate, propagate, coalesce, and intersect during drying, leading to the formation of a complex crack network throughout the soil sample. Other subplots in Tables 5 and 6 (rows “1” to “5”) comparatively demonstrate how desiccation cracks evolve spatiotemporally after each treatment with different fluids.

For samples treated with water (Table 5), the positions and geometries of most cracks change considerably during the wetting-drying cycles, which is consistent with findings obtained by other researchers [45]. Cracks propagate in the three-dimensional space, horizontally to form the coalesced crack network, and vertically to the bottom interface of petri dish plates. With more treatment cycles, the crack connectivity is increased, and soil clods are degraded into smaller and more irregular ones. Comparing three columns in Table 5, for the same cycle number, the extent of cracking reduces with the increasing amount of bottom ashes. It is also interesting to notice that, cracks in sample

A with pure bentonite develop both inside the soil body and along the circumferential boundary. In contrast, cracks in other two samples with bottom ash admixtures are mostly circumferential. This cracking effect corresponds to relatively more integrated soil bodies in samples B and C, which is more apparent within the first few cycles.

Table 5



















Desiccation crack pattern in soils treated with water (group 1)

Cycle No.	Sample A	Sample B	Sample C
	100% bentonite	80% bentonite + 20% bottom ash	60% bentonite + 40% bottom ash
0 (water)			
1 (water)			
2 (water)			
3 (water)			
4 (water)			
5 (water)			

The evolutions of desiccation cracking patterns in MICP-treated soil samples are presented in Table 6. At the end of treatment 0, similar cracking patterns as those shown in Table 5 can be obtained: The largest soil-dish boundary separation occurs in sample B, followed by sample C, whereas sample A is dominated by the crack coalescence within the soil body (row “0”, Table 6). With increasing cyclic MICP treatments, the extent of cracking reduces, as reflected by the narrowing and healing of cracks. Unlike those in water-treated samples, the geometry and morphology of the crack network skeleton in MICP-treated samples experience less changes across different treatment cycles. In comparison to other two samples, the healing effect is more evident in sample C, where the soil body is restored close to its intact state (row “5”, Table 6). We also observe the formation of new cracks, especially crack branches that originate and propagate from primary crack networks. During the wetting-drying cycles, the surface of MICP-treated soil becomes increasingly uneven, implying the calcite precipitations on the soil surface, which is not observed in water-treated samples.

Table 6

Desiccation crack pattern in soils treated with MICP solutions (group 2)

Cycle No.	Sample A	Sample B	Sample C
	100% bentonite	80% bentonite + 20% bottom ash	60% bentonite + 40% bottom ash
0 (water)			
1 (MICP)			
2 (MICP)			
3 (MICP)			
4 (MICP)			
5 (MICP)			

Quantitative characterization of crack patterns. To quantify the evolving characteristics of crack patterns, we carried out image analysis for all crack patterns shown above. Three geometrical parameters including surface crack ratio, average crack width, and total crack length were determined for all samples at the end of each treatment cycle.

Figure 9 shows the evolution of the surface crack ratio values in all samples. After preliminary treatment, samples A, B and C in group 1 (water treatment) have a surface crack ratio of 26.5%, 22.5%, and 14.6%, respectively (Figure 9a). These values are comparable with those obtained at the end of preliminary treatment for group 2 (MICP treatment) (Figure 9b), validating the repeatability of the experiments. The surface crack ratios for all water-treated samples increase with the number of wetting-drying cycles, with the highest value consistently obtained from sample A that is prepared using pure bentonite (Figure 9a). In samples treated with MICP solutions, we observe a parabolic trend that surface crack ratio increases first after treatment 0, reaches the peak value at treatment 1, and then decreases in the subsequent four treatment cycles (Figure 9b). With MICP treatments, sample A with pure bentonite still presents the highest cracking area. As the number of cyclic MICP treatment increases, the surface crack ratio gradually declines and approaches zero. Comparing with treatment 0, the reduction of surface crack ratio at the end of the 5th cycle reaches 65%, 77%, and 91% in samples A, B, and C, respectively.

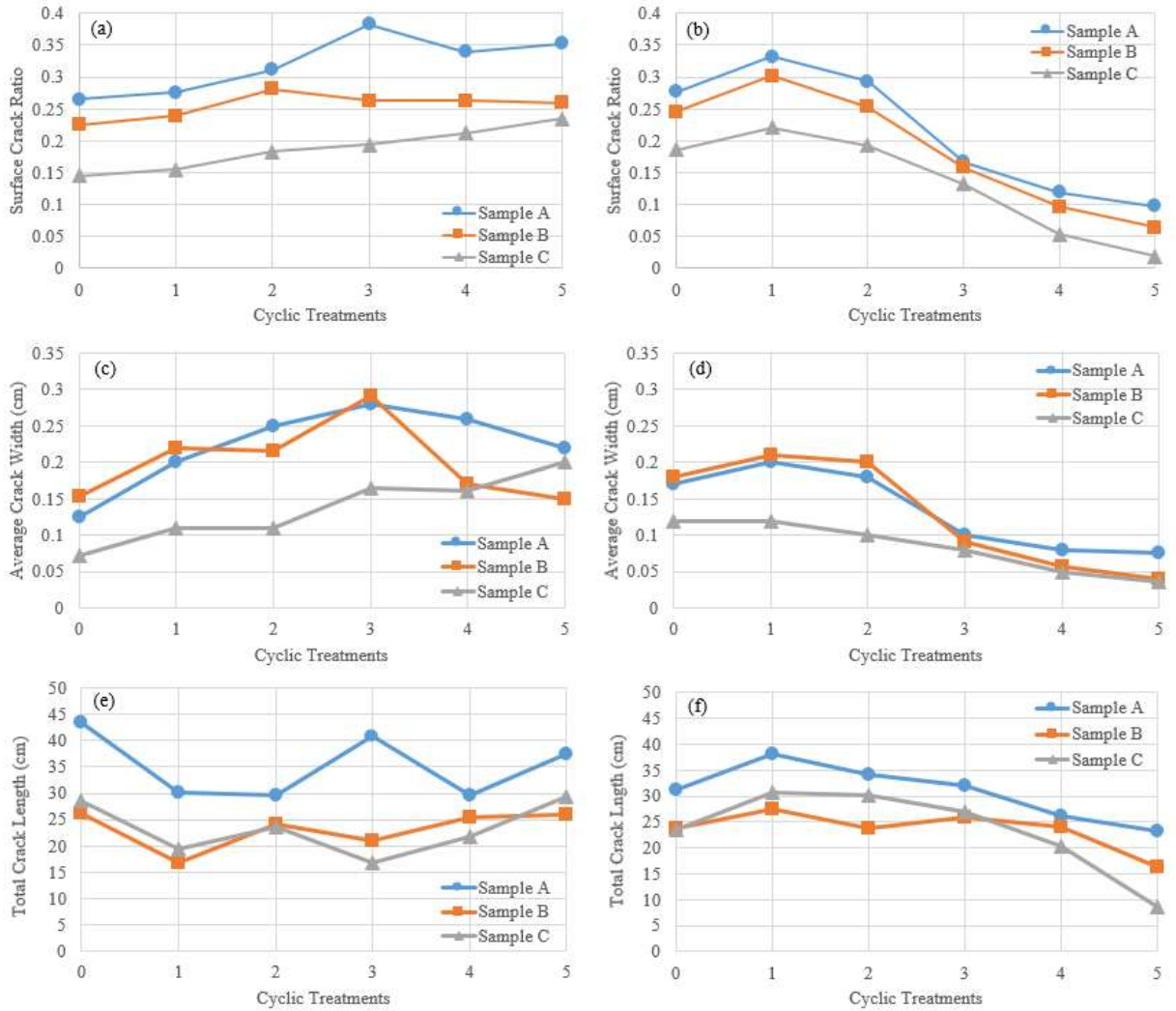


Figure 9. The evolution of geometrical parameters in soil samples (group 1: water-treated samples; group 2: MICP-treated samples) subjected to wetting-drying cycles: (a) surface crack ratio of group 1, (b) surface crack ratio of group 2, (c) average crack width of group 1, (d) average crack width of group 2, (e) total crack length of group 1, and (f) total crack length of group 2.

Although the crack area follows an increasing trend in water-treated bentonite samples, the evolutions of average crack width and total crack length are highly irregular. They seem not to follow any trend (Figures 9c and 9e). Comparatively, both average crack width (Figure 9d) and total crack length (Figure 9f) obtained from MICP-treated samples

exhibit the parabolic trend to a certain extent. At the end of the treatment cycles, the cracks in sample A have a larger dimension characterized by larger width and length values than those in samples B and C. With more cycles of MICP treatments, the bioremediation of soil cracks becomes more evident, as shown by the smaller average crack width and shorter total crack length.

Discussion

Effect of bottom ash admixture on desiccation cracking. The desiccation crack patterns shown in the previous section indicate that, with bottom ash admixture percentage increasing from 0 to 40%, soil samples tend to exhibit less cracking. After five wetting-drying cycles, the surface crack ratios in sample C are much smaller than those in sample A, corresponding to 33.5% reduction under water treatment and 81.1% reduction under MICP treatment. The addition of bottom ash has two significant effects on desiccation cracking. First, bottom ash shows little plastic behavior, implying a very low potential of swelling and shrinkage upon water content changes. In contrast, bentonite soil has a very high plasticity index due to the high plastic montmorillonite minerals (Table 1). Replacing bentonite with bottom ash particles dramatically reduces the overall plasticity index of the mixture. Second, non-expansive bottom ash particles are capable of reducing the shrinkage potential of clay particles. The bottom ashes are primarily composed of non-crystalline silicate, calcium, aluminum, and iron oxides compounded with some microcrystalline material (Table 4). These bottom ashes have the potential to provide multivalent cations such as Ca^{2+} , Al^{3+} , Fe^{3+} , which promotes the flocculation of clay particles by cation exchange. As a result, the surface area and water affinity of the soil samples decrease, implying a reduction in the shrinkage potential. However, bottom ash cannot

fundamentally eliminate soil cracking. At 40% bottom ashes in the mixture, desiccated soils still generate increasing cracking as the cyclic wetting-drying conditions continue (Figure 9a).

At the end of the cyclic treatment, SEM images were taken to characterize the microstructural changes in these desiccated samples. Unlike small spherical fly ash particles [51], bottom ash particles are larger and have more angular shapes (Figure 10c). During wetting-drying cycles, high plastic clay deforms significantly, whereas low plastic bottom ash aggregates show minor deformation. This is the main cause to the formation of local stress concentrations at the ash-soil interface, which drives the opening and propagation of micro-cracks in the soil body.

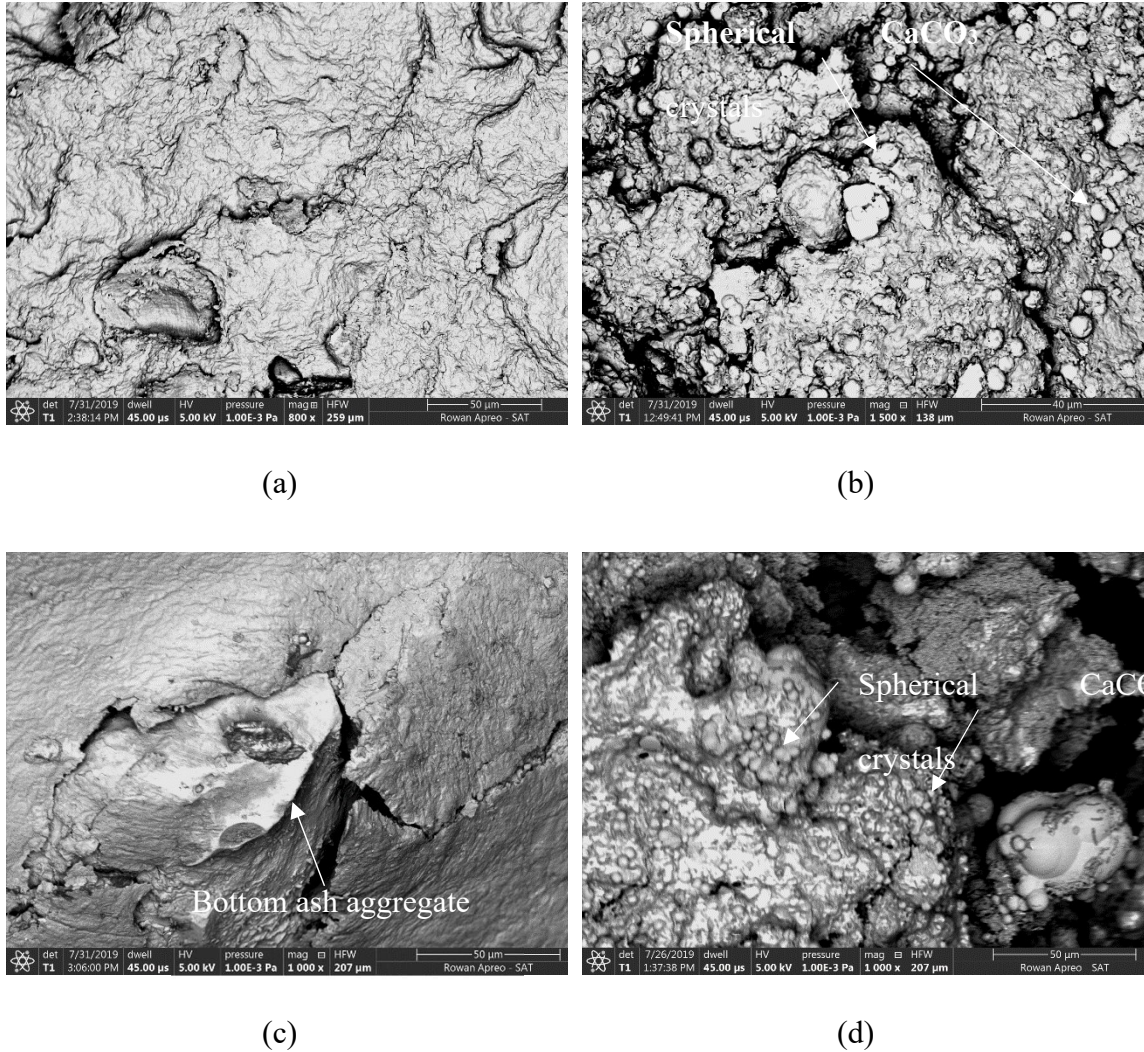


Figure 10. SEM images of soil samples at the end of five cycles of treatments: (a) sample A under water treatment; (b) sample A under MICP treatment; (c) sample B under water treatment; and (d) sample C under MICP treatment.

Effect of fluid type on desiccation cracking. In this study, the soil desiccation cracking behavior is governed by two competing mechanisms: (1) Water evaporation in bentonite decreases the pore pressure and induces matrix suction, which acts on the soil skeleton and drives the crack opening once it exceeds the tensile strength of soil [7, 52]; and (2) Calcite precipitation enhances the inter-particle bonding and resists cracking [53].

In all water-treated samples (group 1), the first mechanism dominates, resulting in the development of desiccation crack patterns under drying conditions (Figure 9a). The crack segments are smooth and mostly form an intersection angle of 90-150 degrees. This is consistent with the observations by other research [52, 54], and can be interpreted using the maximum stress release and crack propagation criterion [44]. Upon wetting, the original desiccation cracks tend to be increasingly narrow due to the filling of the exfoliated soil aggregates from the clods as well as the volume swelling of the clods [45]. Repeated volumetric swelling-shrinkage and the resulting cracking during the wetting-drying process lead to irreversible soil fabric changes and the degradation of structural integrity in the soil sample.

Based on quantitative and qualitative comparisons in the results section, MICP treatment yields a promising influence on crack remediation. Mixing the cementation solution with the bacteria solution yields the precipitation of numerous spherical CaCO_3 crystals of similar size, well-distributed spatially (Figures 10b and 10d). These crystals formed on the vertical surface of crack are able to bond the adjoining soil clods together and fill up the inter-granular space, which improves the tensile strength of soil around the cracks [18]. Calcite precipitations in the vicinity of particle contacts also serve as an additional bonding agent to soil particles, contributing to the increase of soil strength and the improvement of cracking resistance. Due to the usage of the surface spraying method, MICP reactions occur not only inside the crack, but also on soil surface. This explains the presence of CaCO_3 crystals on the sample surface (Table 6), resulting in the formation of increasingly uneven soil profiles with more treatment cycles. Without calcite precipitations, water-treated samples in group 1 have relatively flat surfaces (Table 5).

Certain surface heave and settlement deformations can be observed in these samples (Figure 10a), which can be attributed to the repeated soil expansion and shrinkage during wetting-drying cycles. The detailed cracking behaviors of MICP-treated samples are determined by the interplay of crack driving force and bio-cemented soil strength. The wetting of MICP-treated samples is associated with crack closure and healing, originated from the coupled effect of soil swelling and bio-cementation. Note that, because of the soluble calcium cations provided by calcium bentonite and bottom ash, the addition of MICP solutions leads to an enhanced hydrolysis reaction and a better biocementation effect [55]. The individual contribution of calcium bentonite and bottom ash to calcite precipitation will be analyzed in future investigations.

Effect of treatment cycle number on desiccation cracking. To quantify the cracking resistance of soils at different cycles, we adopted the concept of crack reduction rate (R_{cr}) that was first introduced and applied in the study of fiber-reinforced soil by Miller and Rifai [53]:

$$R_{cr} = \frac{R_{sc,u} - R_{sc,ti}}{R_{sc,u}} \times 100\% \quad (4.1)$$

where $R_{sc,u}$ is the surface crack ratio of the soil specimens at the end of preliminary treatment. $R_{sc,ti}$ is the surface crack ratio of the soil specimens after each cyclic treatments, with i varying from 1 to 5.

The crack reduction rates obtained for soil samples in group 1 remain negative throughout the cyclic treatment (Figure 11a), indicating the increasing crack area after preliminary treatment. Soil shrinks under drying and swells under wetting conditions. The cyclic wetting-drying process leads to the formation of irreversible soil microstructural

changes and the creation of many weak zones, which significantly controls the onset positions of cracks in the subsequent cycles. This explains why, as the cycle number increases, we observed both the re-opening of cracks generated in previous cycles and the initiation of new cracks in the neighboring regions (Table 5).

As shown in Figure 11b, for MICP-treated samples, the crack reduction rate increases from negative to positive values with the increasing wetting-drying cycle number, which highlights the competing effects of crack driving force and crack resistance force. After the 1st cycle, all samples have negative crack reduction rate, implying an increment in the crack area, which is attributed to the insufficient MICP solutions for biocementation. With more cycles of treatments, the newly formed crystals precipitate on crystals produced in previous treatment cycles. The gradual accumulation of crystals increases the size of crystal clusters and causes the cementation between adjacent clusters [55]. The densely distributed CaCO₃ crystal clusters on soil particle surface and inside inter-particle pores contributes primarily to the improved mechanical integrity of soil samples. Therefore, with more MICP treatments, soil samples exhibit stronger resistance to cracking under drying, reflected as higher crack reduction rate (Figure 11b) and smaller crack dimensions (Figures 9b, 9d, and 9f). Due to the continual precipitation of calcite crystals on the soil surface, the surface roughness of MICP-treated samples increases with the treatment cycle (Table 6). The formation of the surface film hinders the penetration of water during wetting and the loss of moisture during drying, resulting in a possible reduction of capillary suction in soils.

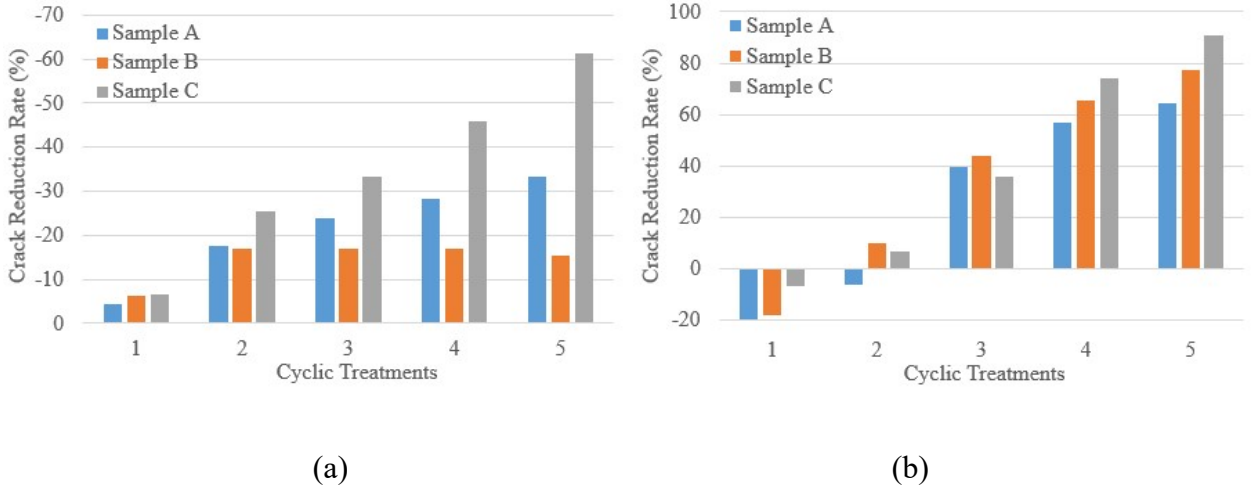


Figure 11. The evolution of crack reduction rate with wetting-drying cycles: (a) water treatment; (b) MICP treatment

Summary of Findings

To investigate the potential of using bottom ash and MICP for the remediation of desiccation cracking in clayey soils, we performed a series of cyclic wetting-drying tests on laboratory-scale soil samples. Two groups of bentonite samples mixed with different percentages of bottom ashes were treated with water and MICP solutions, respectively. The qualitative and quantitative analyses of soil cracking behaviors lead to the following conclusions:

- 1) The addition of bottom ash into clayey soils reduces the plasticity of the mixture and promotes the flocculation of clay particles by cation exchange, which jointly contributes to the reduced shrinkage potential and desiccation cracking of soils. The soluble calcium cations provided by bottom ash adds to the enhanced hydrolysis reaction during the MICP process and results in a better biocementation effect.

2) Water-treated soil samples experience volume swelling and shrinkage, crack opening, propagation, coalescence, closure and healing under wetting-drying cycles. Quantitative analysis results based on image processing reveal that the crack area in water-treated samples monotonically increases with the wetting-drying cycles, which can be attributed to the irreversible soil fabric changes and the degradation of structural integrity in the soil sample.

3) MICP treatment is effective in remediating desiccation cracks, with the effect governed the interplay of crack driving force and bio-cemented soil strength. The parabolic evolution of crack geometrical parameters including surface crack area, average crack width, and total crack length indicates that calcite precipitations are insufficient to resist cracking in the first cycle of treatment and gradually increase with the subsequent treatments. The densely distributed CaCO_3 crystal clusters on soil particle surface and inside inter-particle pores contributes primarily to the improved mechanical integrity of soil samples.

The study highlights the potential of using bottom ash and MICP in reinforcing clayey soils for cyclic wetting-drying conditions. The inclusion of bottom ash admixtures contributes to the recycled usage of waste materials and reduces the desiccation cracking in clayey soils. The surface spraying of MICP solutions is easy to operate and provides a new possibility for field-scale implementations. Future studies will focus on the optimization of surface spraying methods and the bio-remediation of heavy minerals in bottom ashes through MICP. The bio-stabilization of clayey soils explored in this study brings new insights into the remediation of soil erosion and cracking for various climate changes, which is key to the design and performance of sustainable infrastructures.

Chapter 5

The Analysis of the Remediation of Desiccation Cracking of Sandy Clay with the Addition of Bottom Ash Admixture through Digital Image Correlation

Methodology

Understanding the formation and propagation of desiccation cracking can be a useful technique while evaluating crack remediation. Networks of desiccation cracking can be studied directly through Digital Image Correlation (DIC). Analyzing the formation of the crack networks through real time displacement can be used to predict future crack networks and quantify the desiccation cracking behavior of sandy clay (Table 7) mixed with bottom ash admixture (Table 4).

This soil represents potential in field soil and allows for the analysis of the feasibility of adding bottom ash admixture into clayey soils prone to desiccation cracking. One of the most significant benefits of using bottom ash is allowing an abundant waste material to be recycled, thus creating an added value to this by-product. Bottom ash has shown promise in remediating desiccation cracking in Bentonite (Chapter 4) and it is important to determine the impact bottom ash can have on natural soil.

Table 7

Characteristics of sandy clay gathered from Tech Park

Soil Properties	Value
Specific Gravity	2.39
Liquid Limit (%)	22.7
Plastic Limit (%)	13.2
Gravel (%)	0
Sand (%)	30%
Below #200sieve	70%

Test setup. Figure 1 shows the schematic of the experimental setup in this work. Images were captured from the speckled surface of samples during drying using a Rebel t6i camera. The camera lens was positioned above and perpendicular to the exposed surface. The sample was placed atop a scale to enable the real-time recording of its mass loss due to drying. Images were continuously recorded at 30 minute time intervals. A high intensity LED light was used to illuminate the sample surface. The entire setup was placed inside a blackout cover to reduce the effects of ambient lights.

Sample preparation. This study investigates three soil samples of sandy clay; sample 0%BA, Sample 20%BA, and Sample 40%BA Bottom ash is hand-mixed into the sandy clay with a moisture content of 50%. This is roughly 1.5 times the liquid limit of the soil (Table 7). The wet soil is then placed wet in 5cm petri dishes to limit voids between the soil and petri dish.

Imaging and digital correlation. Deformation and strain fields developed in the samples during drying were characterized in situ by digital image correlation (DIC) measurements. To use DIC in the present work, the exposed surface of the wet sample was coated with a thin layer of matt black paint that was sprayed directly on the surface of interest. To ensure that the speckle pattern does not affect the drying process, several independent measurements were conducted wherein the drying kinetics of samples with and without the pattern were compared. These independent measurements revealed that the drying kinetics are not affected by pattern deposition likely because of the discontinuous nature of the coating that leaves enough channels for the drying process.

Images captured during drying were analyzed using the commercial DIC software Vic-2D (Correlated Solutions, Inc.). In this software, the DIC area of interest (AOI) was selected as a circular region with a diameter of approximately 1700 pixels ($\sim 29 \mu\text{m}/\text{pixel}$ resolution). The in-plane strain fields developed during the drying process were quantified using subset and step sizes of 49 pixels and 7 pixels, respectively. A strain filter size of 5 was used for full-field strain measurements. This strain filter size is equivalent to a virtual strain gage (VSG) of $\sim 200 \mu\text{m}$ that facilitates the measurement of highly localized strains with sharp gradients in the vicinity of the cracks.

The image correlation parameters were selected to ensure a full correlation while keeping the strain noise floor at a minimum [38]. Figure 12 shows the DIC area of interest and the subset size used. Strain bias and noise floor were characterized based on the procedure detailed in [56] and using a set of at least 5 stationary images captured before the onset of the experiments. Strain bias and noise floor in this work were determined as -5.74×10^{-5} and $10.7 \times 10^{-5} \mu\epsilon$, respectively. The strain noise floor determined here is at least

5 orders of magnitude lower than strains measured during the drying process. The shrinkage-induced out-of-plane motion of the sample surface was neglected due to its insignificant contribution to the in-plane deformation fields [57].

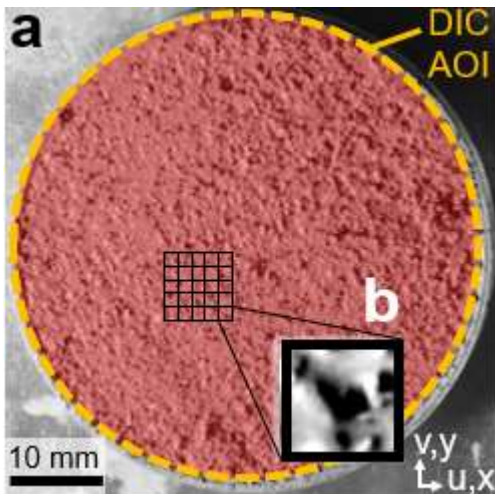


Figure 12. DIC Area of Interest

Results

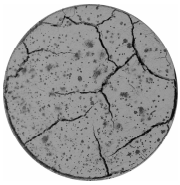
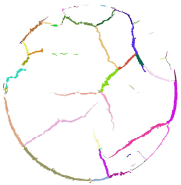

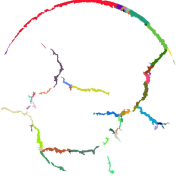

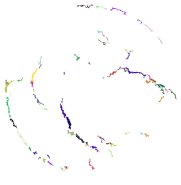
Water evaporating during drying. Using CIAS, different crack parameters could be studied including crack area, average crack width, and total crack length (Table 8). It can be visually observed and quantitatively proven that the addition of bottom is effective in remediating desiccation cracking. Visually it is easy to see that Sample 40%BA and Sample 20%BA have less crack area than Sample 0%BA and that bottom ash limits crack formation and potential. The heavy metals in the bottom ash expose the soil to cation exchange and limit the potential expansion of the soil. The structural integrity of the soil sample is maintained as moisture loss occurs. Moisture loss over time is shown in Figure

13. As the initial rate of moisture loss is consistent in all three samples, Sample 40%BA and Sample 20%BA begin to plateau much sooner than Sample 0%BA. The plateau results in a higher final moisture content for sample 40%BA. This higher moisture retention correlates directly with crack area as the less moisture evaporated results in less desiccation cracking.

The plasticity reduction in the soil can also be shown through the analysis of average crack width and total crack length. Average crack width may be more dependent on the number of crack segments obtained through image processing or the outlier of larger shrinkage cracks may skew the average resulting in 20%BA having a higher average crack width than 0%BA, however it can be seen in the 40%BA sample that crack expansion is limited by the addition of the bottom ash admixture, and that is represented through the lowest average crack width of 0.18 cm. Total crack length displays clearer evidence that bottom ash remediates desiccation cracking with 0%BA having the highest total crack length as 40%BA has the lowest. This trend shows bottom ash's ability to prevent crack propagation and disrupts crack networks from forming. The addition of bottom ash helps retain the structural integrity of the soil body and less cracking results in a less permeable clay.

Table 8

CIAS Results

Sample	24 Hour Image	Crack segments	Crack area (%)	Average Crack Width (cm)	Total Crack Length (cm)
0%BA			7.76	0.028	38.58
20%BA			6.86	.053	26.12
40%BA			2.44	0.018	17.49

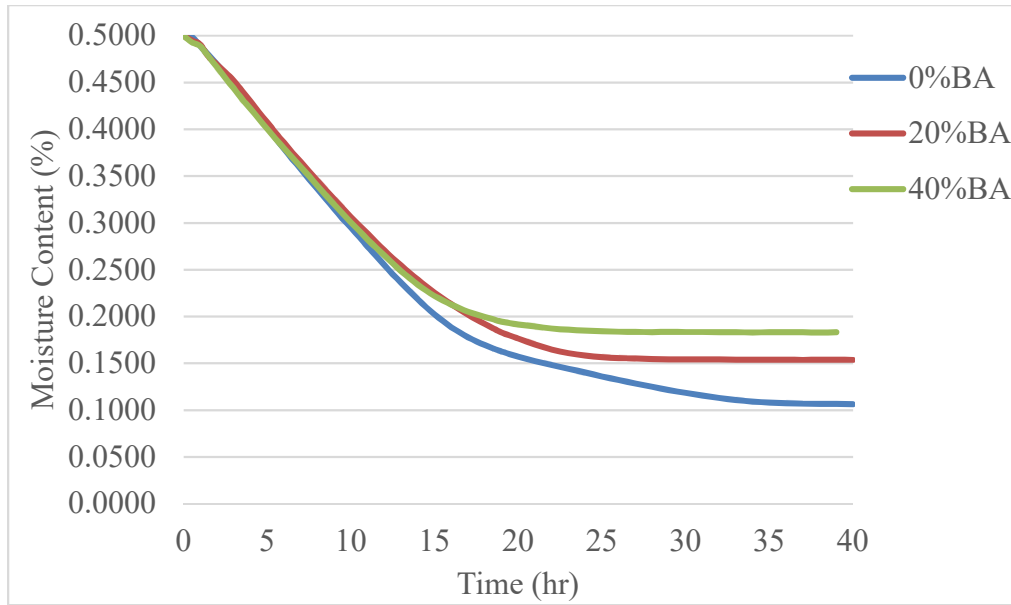


Figure 13. Moisture Content Over Time

Volumetric shrinkage during drying. Digital image correlation gives further insight into the desiccation cracking process and the remediation impact bottom ash can have on clayey soils. Figures 14, 15, and 16 show the radial displacement of all three soil samples over time and the red color indicates 0 radial displacement [38]. The color brightens as radial displacement increases and this represents the shrinkage of the soil sample. The shrinkage begins near the edge of the petri dish as the colors brighten around the edges of all three samples. Early displacement predicts future cracks before initial cracking has begun This is evident in all three samples as the edges become brighter within the first few hours, and this brightness begins to move toward the soil body indicating displacement of the soil particles [56]. The soil particles begin to separate resulting in crack formation and potentially the formation of an entire crack network. All maximum displacements occur near the boundary in all three samples, and this shows the impact the

petri dish has on each sample. This impact appears consistent and does not affect crack area measurements.

Another trend observed is red area appearing near crack tips in all three samples. As cracks form the displacement near the crack is tips is 0 due to the compressive inward stress of the neighboring and the fixed boundary of the nearby crack. Sample 0%BA at 3.5 hours has many red areas around the forming crack network. As time continues the red area decreases indicating the inward displacement of non-cracked or intact soils. The end of cracking results in smaller red areas surrounding the propagated crack networks. Radial displacement measurements can also show the impact of bottom ash admixture. The scale for sample 40%BA is significantly lower than the other two samples showing again the limited potential of soil expansion and crack propagation. Sample 40%Ba experiences less radial displacement, and therefore has the more intact soil body[37]. Shrinkage cracking is severely limited indicating there is less capability for the soil to be pulled inward.

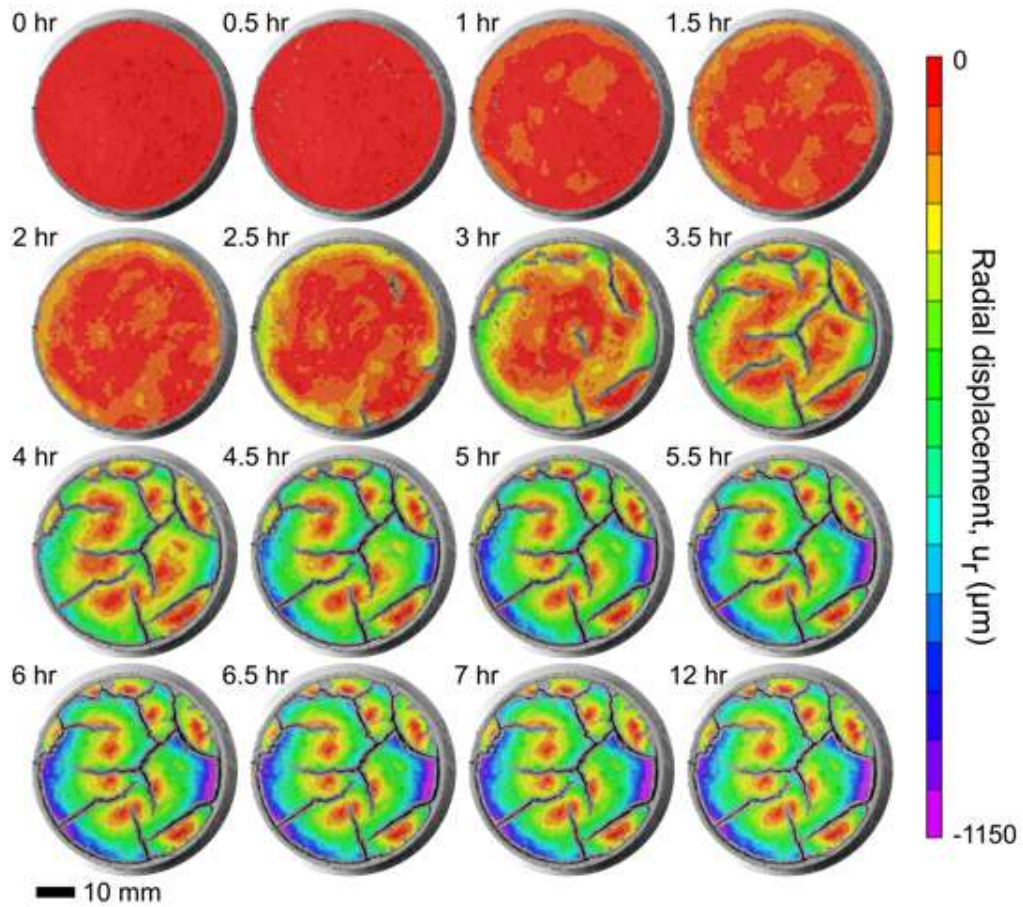


Figure 14. Contour maps showing the evolution of radial displacement at various time steps during drying of 0% BA sample. No significant change is observed after 7 hrs.

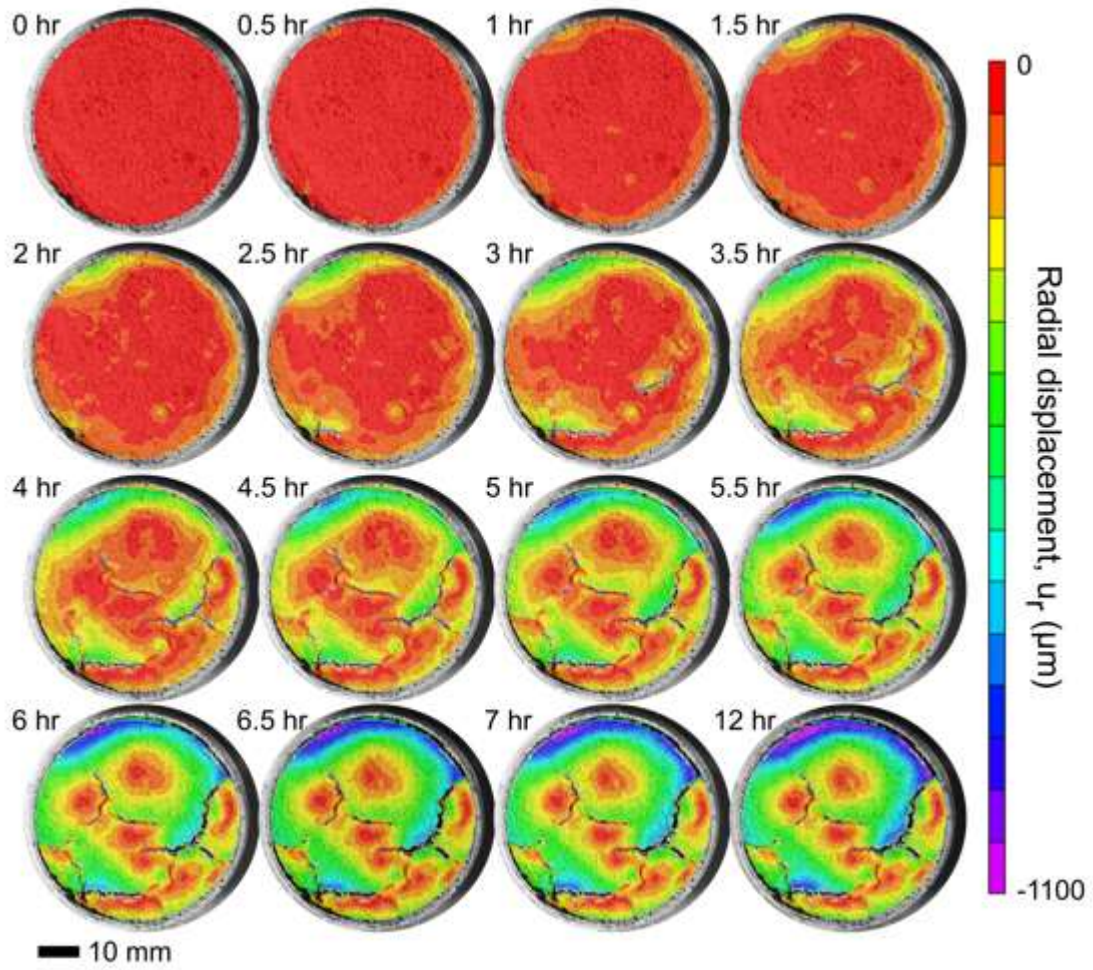


Figure 15. Contour maps showing the evolution of radial displacement at various time steps during drying of 20% BA sample. No significant change is observed after 7 hrs.

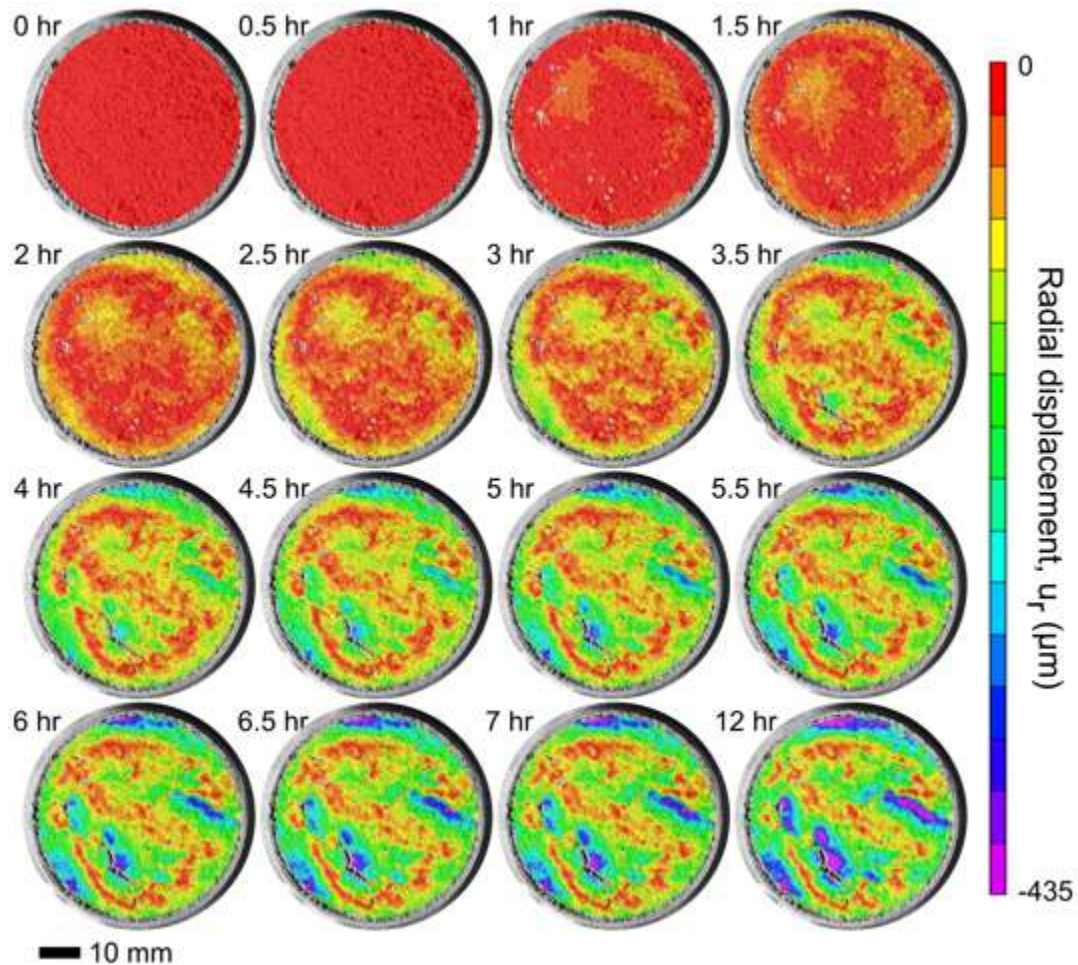


Figure 16. Contour maps showing the evolution of radial displacement at various time steps during drying of 40% BA sample. No significant change is observed after 7 hrs.

Minor principle strain. Another parameter being measured is minor principal strain. This is a measurement of strain due to the tensile forces of evaporation leading to desiccation cracking. The minor principal strain over time is shown in Figures 17,18, and 19. Again, the red color indicates 0 strain, therefore each initial sample at 0 hour is completely red. The sample brightening up indicates strain is occurring. Similarly, to radial displacement, initial strain is seen around the edges of the petri dish or the soil boundary and over time this strain occurs throughout the soil body indicating where future cracks

will form. There is much clearer disparity between the three samples in terms of minor strain. Sample 0%Ba experiences strain throughout the entirety of the sample as Sample 20%Ba and 40%BA have larger red areas indicating 0 displacement. The impact of the bottom shows portrays that there is a resistance to displace in sample 20%Ba and 40%BA. There is significantly less displacement throughout the soil body in the bottom ash samples.

Maximum strain occurs near the cracks due to the separation of soil particles and this is consistent with all three samples. Sample 40%Ba has minimal high strain areas due to the addition of bottom ash as Sample 0%BA has high strain throughout the entire soil body resulting in multiple crack networks. The consistency of these high strain areas indicate heterogeneity [37]. Heterogeneity shows when displacement becomes consistent or shows no change over time. Sample 0%BA is able to obtain heterogeneity at approximately 5 hours, sample 20%BA occurs at 6 hours, and sample 40%BA occurs at 7 hours. Bottom ash delays maximum strain and keeps the soil body intact and this is evident through a smaller maximum minor principal strain compared to Sample 0%BA and 20%BA.

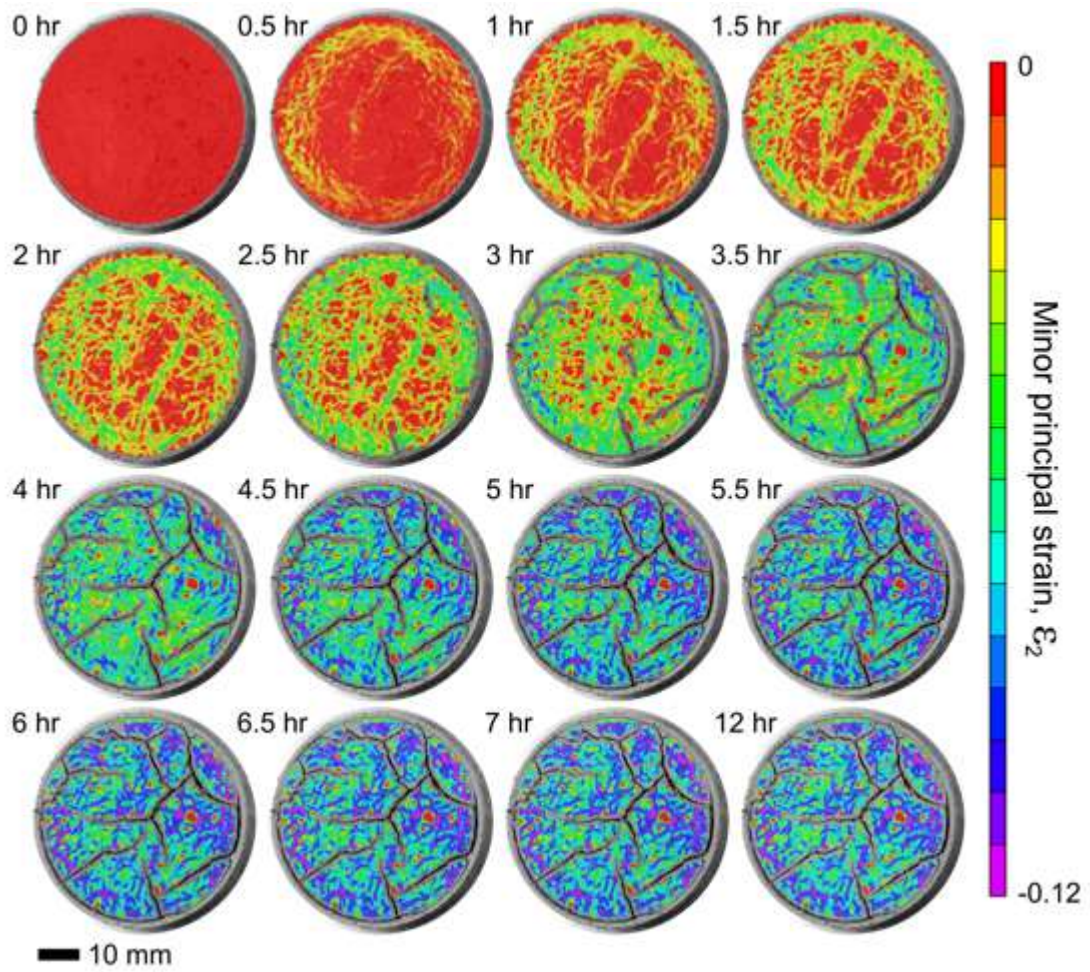


Figure 17. Contour maps showing the evolution of the second principal strain (ϵ_2) at various time steps during drying of 0% BA sample. No significant change is observed after 7 hrs.

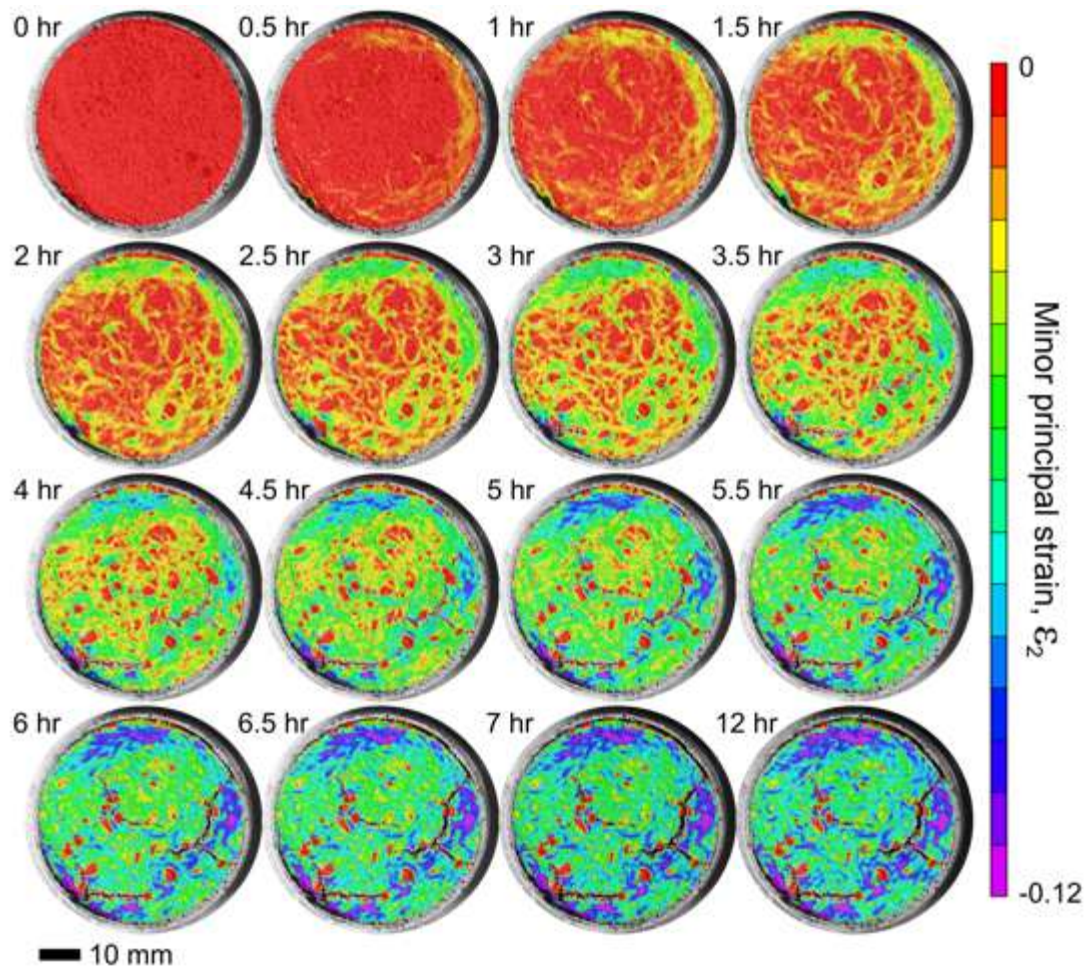


Figure 18. Contour maps showing the evolution of the minor principal strain (ϵ_2) at various time steps during drying of 20% BA sample. No significant change is observed after 7 hrs.

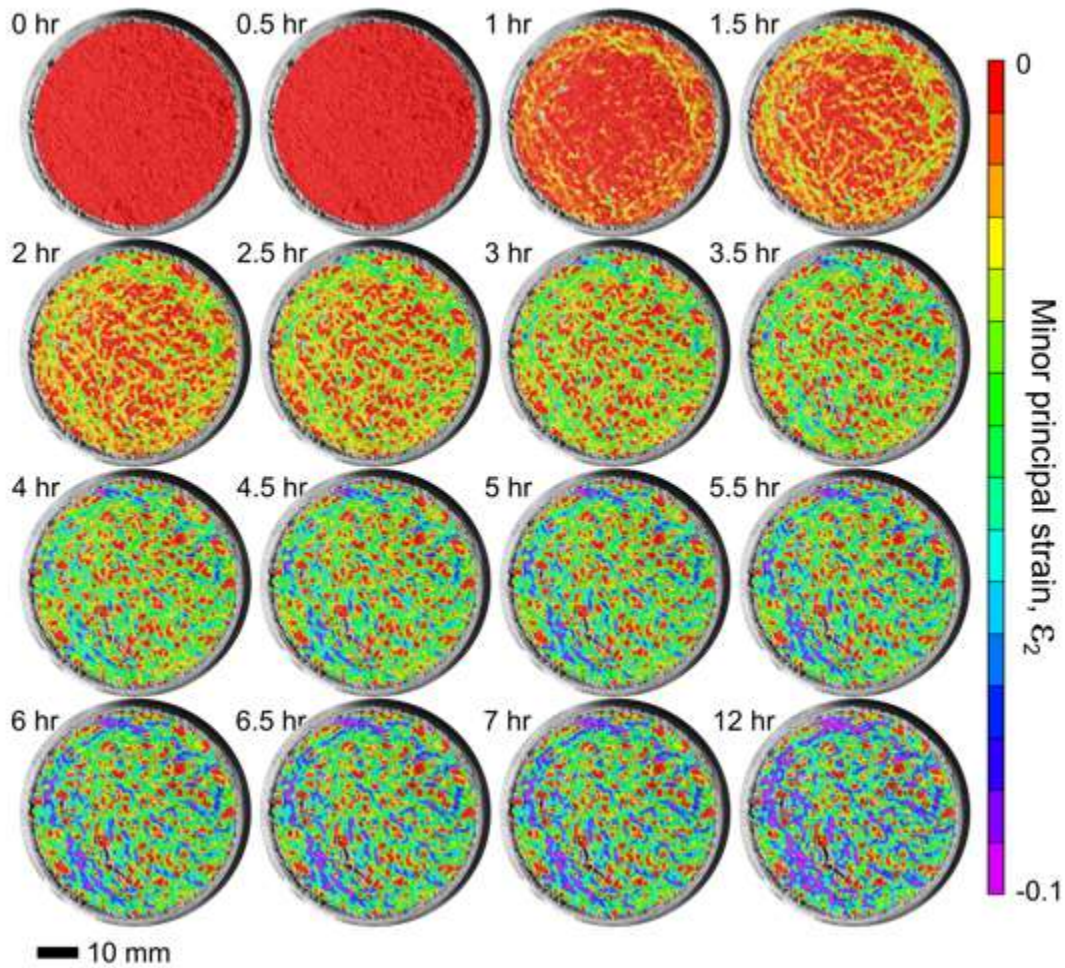


Figure 19. Contour maps showing the evolution of the minor principal strain (ϵ_2) at various time steps during drying of 40% BA sample. No significant change is observed after 7 hrs.

Discussion

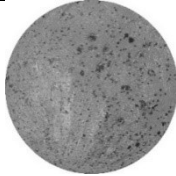
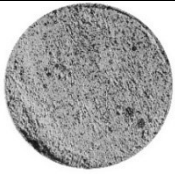

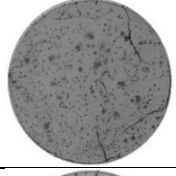
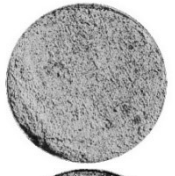

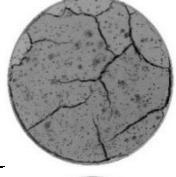


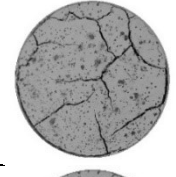
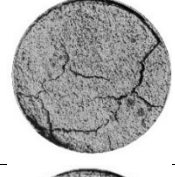
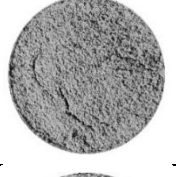
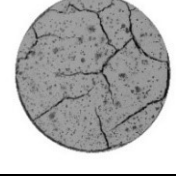

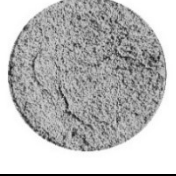
Crack area confidence intervals. Confidence intervals show major differences among all 3 samples. The difference of Sample 0%BA is 0.693, Sample 20%BA possesses a difference of 0.554%, and sample 40%BA possesses a difference of 0.416%. This indicates there is no significant difference in terms of crack area regarding Sample 0%BA and Sample 20%BA. Sample 40%BA possesses a significant difference within the

confidence interval range of all three samples. 20%BA may not have a significant impact in terms of crack area remediation; however Sample 40%Ba shows major improvements in remediating impacts on cracking area. Future studies should look to further optimize the percentage of bottom ash to maximize the remediation impacts of bottom ash admixture.

Effects of bottom ash. The addition of bottom ash admixture into sandy clay reduces desiccation cracking and changes the soil's surface morphology. The added plasticity and size of the bottom ash soil particles reduces the potential of soil expansion. Microcracks form around the bottom ash particles resulting in an increased surface roughness. Table 9 shows the crack propagation over time and sample 0%BA experiences appears to have a much smoother soil surface compared to the bottom ash samples, but also develops cracks faster and to a greater extent. Bottom ash limits crack network expansion as cracks are unable to join and coalesce throughout the entire sample. Soil roughness should be studied further using 3d analysis or high-resolution imaging.

Table 9

Crack Propagation over time

T (hr)	Sample 0%BA	Sample 20%BA	Sample 40%BA
0			
3			
6			
12			
24			

Area of interest comparison. DIC allows some insight into the soil surface characteristics with the ability to isolate intact soil with no cracks from the entire soil body and compare this smaller area of interest to the larger area of interest or entire sample [38]. The entire AOI and isolated intact soil body AOI is compared as seen Figure 20. The comparisons within these areas of interest is vital to understanding the strain that is

occurring within the soil samples. Figure 21a and Figure 21b show that sample 40%BA has significantly less minor principle strain in both areas of interest. This insight shows how the soil is affected as cracks form and how intact soil responds to shrinkage or cracks forming around it around it.

An interesting analysis is the direct comparison between the full scale AOI and the crack free AOI. The initial rate of strain occurring is consistent with all three samples and in both areas of interest. This is consistent with the drying process shown in Figure 14. Initially all samples experience a similar initial evaporation process. Samples begin to differ around the 4-hour mark and the rate of displacement significantly slows in the bottom ash treated samples, and Sample 0%BA strain rate increases until plateauing around 5 hours. These trends are consistent in both areas of interest. An interesting observation is the 20%BA and 0%BA have very similar strain curves with 20% showing overall less strain and a slower rate of strain. These curves are linear until reaching their plateau, but Sample 40%BA experiences a change in strain rate before plateauing. This highlights the effects of the reduced plasticity of the soil and the success of cation exchange within the soil matrix.

This behavior is essential to the structural integrity of the soil and it is clear that Bottom ash significantly delays strain throughout the soil sample. Sample 0%BA possesses similar results in both areas of interest considering there is nothing holding back the shrinkage of the soil. Sample 0%BA reaches its max strain at nearly 5 hours and then begins to plateau. The full area of interest shows less displacement in the Bottom Ash treated samples, and longer time for the strain to plateau as 20%BA plateaus at nearly 7 hours and

40%BA plateaus at nearly 9 hours. This delay and limitation of minor strain shows the increased durability and strength of the bottom ash samples.

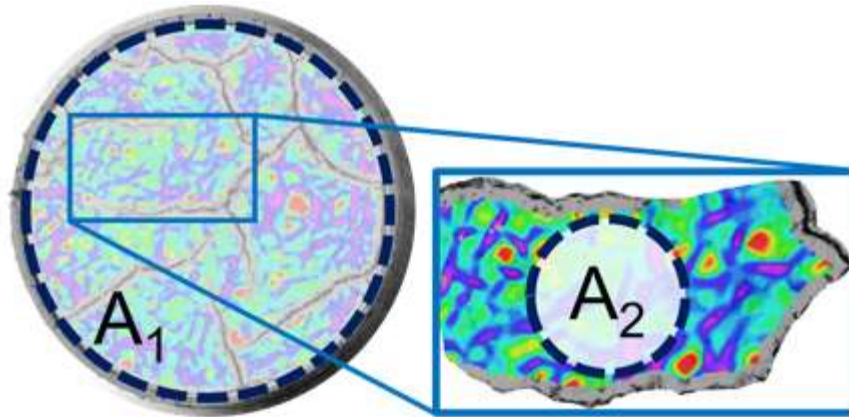


Figure 20. Full, A₁, and reduced, A₂, AOIs are shown for a 0% B.A. sample.

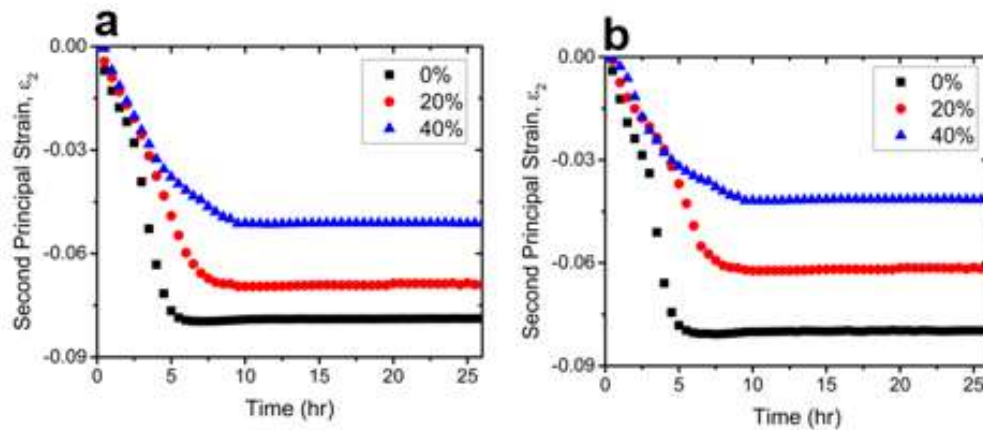


Figure 21. Variation of second principal strain, ϵ_2 , with respect to time for samples with 0%, 20%, and 40% B.A., extracted for (a) full DIC AOI, and (b) Reduced (crack-free) AOI.

Summary of Findings

This study investigated the remediation capabilities of bottom ash admixture when added to sandy clay through image processing and digital image correlation. Three Samples (0%BA, 20%BA, 40%BA) underwent desiccation cracking tests and photos were taken every half hour to obtain the crack morphology and water loss over time. These results lead to the conclusions of;

1. The addition of bottom ash admixture leads to significantly less moisture loss in sandy clay resulting in less desiccation crack area (Figure 14 and Table 8). Bottom ash limits the potential of expansion and shrinkage of the soil specimen and prevents the formations of crack networks through cation exchange and reducing the plasticity of the soil.
2. Analysis using Digital Image Correlation gives valuable insight into the formation of crack networks, and crack initiation. Initial radial displacement occurs near the edge of the soil sample and continues inward toward the soil body. Future cracks can be predicted based on these initial results. Sample 40%BA has significantly less radial displacement or shrinkage due to the addition of Bottom ash. This further proves the positive impacts of bottom ash has on remediating desiccation cracking. The sandy clay particles have less shrinkage or expansion potential in samples with bottom ash admixture (Figures 15.16,17). Sample 0%BA has no resistance and an entire crack network is able to form throughout the entire soil body. The addition of bottom ash keeps the structural integrity of the soil intact.
3. DIC is also able to measure the minor principle strain throughout all the three samples and through isolated crack free area of interests. This analysis shows the limited strain of sample 40%BA and significantly less soil expansion. Bottom ash add roughness to the soil

as microcracks form around bottom ash particle, however Sample 0%BA has a much smoother surface but a much more extensive crack network. Analyzing smaller intact soil areas shows how the soil is impacted despite not having any cracks. Sample 40%BA shows much less strain delays final crack propagation. Sample 0%BA has strain occur at a consistent rate and reaches its ultimate strain much faster than the bottom ash treated samples. The addition of bottom ash delays crack propagation and limits the minor principle strain occurring within the soil sample.

This study focused on the remediation of desiccation cracking of field applicable sandy clay with the addition of bottom ash admixture. The use of digital image correlation allows for new evidence of remediation and soil behavior. These findings are useful to preventing future cracks and predicting potential crack networks before they form. Bottom ash admixture is very effective in remediating desiccation cracking in clayey soils.

Chapter 6

Conclusions

This thesis focuses on the remediation of desiccation cracking in clayey soils. The remediation of desiccation cracking remains an essential problem in geotechnical engineering and this paper highlights the remediation techniques of the addition of MICP and admixture bottom. This analysis is conducted on bentonite clay (Table 1) and sandy clay (Table 7) in the lab scale. The findings throughout this study encourage future work in the field scale development of these remediation techniques and for more in depth tools for comparison such as a 3d scanner of a 3-dimension digital image correlation. The major findings are summarized below.

1. Microbial induced calcite precipitation reduces desiccation cracking area in bentonite clay when hand mixed. The increased bonding strength of the soil reduces crack propagation and limits soil expansion throughout the entire sample. This is shown through higher water retention and later initial cracking. The hydrolysis of the urea and the biocementation effect lead to high moisture retention in MICP treated samples. MICP affects are seen in terms of surface crack ratio and average crack width. Sample 50B50C yielded the lowest crack area showing the optimized solution of MICP solution. Sample 25B75C and sample 75B25C each yielded similar crack ratios and similar average crack widths. The MICP treated samples have an average width of 0.18 cm as Sample W had an average width of 0.28 cm. This difference shows the limited crack potential and soil expansion once MICP treatment is added.

2. The probability distribution of crack areas shows that MICP treated samples are much less likely to experience large desiccation cracks but are more likely to achieve smaller crack areas. Sample W has the highest likelihood to experience large crack areas. This distribution shows the impacts of MICP in remediating desiccation cracking. A similar trend is observed when analyzing crack width. The avoidance of large crack formation allows for the structural integrity of the soil to be maintained and increases the serviceability of the soil. The positive impacts of MICP solution allow for further investigation into its remediation effects and to further advance this technique.

3. MICP injection treatments are effective in remediating desiccation cracking. As treatments increase, the bio cementation effect overcomes the expansion caused by the drying process. The effect leads to a higher structural stability of the soil and can be shown through the analysis of surface crack ratio and average crack width. Water treated samples experience a monotonical increase of crack area with each cycle. Crack reduction rate shows MICP treated samples reduce cracking by nearly 80% as water treated samples experience a negative crack reduction rate. The structural stability of water treated samples is significantly decreased as treatments continue. The addition of MICP can reverse this trend and repair or lessen desiccation cracking to extend the service life of the soil. Further advancement into the field scale investigation of the MICP application is needed due to the lab scale success in remediating desiccation cracking.

4. Bottom ash admixture is effective in remediating desiccation cracking by reducing the plasticity of the soil and promoting cation exchange among the clay particles which leads to flocculation and agglomeration of the clay particles. The addition of bottom ash severely limits the expansion potential of the soil, and this is shown as Sample C with 40% bottom

ash has the lowest crack area. The structural stability of the soil is increased as the addition of bottom ash allows for the soil body to remain mostly intact. Circumferential cracking is mostly observed among the bottom ash treated samples, as Sample A shows the formation of crack networks occurring throughout the entire soil body. Bottom ash also has a visible impact on the surface roughness of the soil resulting in a less smooth surface. This common waste material is effective in remediating desiccation cracking and also provides soluble calcium ions to aid in the MICP reaction. MICP treatments and the addition of bottom ash admixture are able to nearly fully reduce desiccation cracking as Sample C shows a final crack area of only 3%.

5. Digital image correlation is a valuable tool in analyzing soil behavior and crack formation. The real time strain and displacement measurements allow for insight into the initial cracking process and the ability to predict future crack formations. DIC analysis is also able to show the remediation effects of bottom ash admixture in sandy clay. Measuring radial displacement in all three samples showed sample 40%BA experiences the least expansion among all samples, as the max displacement is significantly less than the other samples tested. Insight into soil behavior during the drying process indicate displacement begins at soil petri dish boundary and slowly encircles the entire sample until the cracking process begins. Soil behavior once cracking occurs is also beneficial to the integrity of the soil. As cracking occurs the soil nearest the crack will experience minimal displacement, and further away from crack networks shows higher displacements.

This study was successful in remediating desiccation cracking through the addition of MICP solution and bottom ash admixture. Quantitative analysis was conducted studying observed crack patterns and soil behavior allowing for many findings to be obtained.

Further advancement of this research includes the addition of 3-dimensional analysis using a 3d scanner or 3d DIC. Noticeable changes occur on the soil surface during the drying process and that quantitative analysis is unavailable with a 2-dimensional study. This research provides valuable insight into soil behavior and the formation of crack networks in hopes to remediate the effects of desiccation cracking in clay soils.

References

- [1] R. Pusch, "Highly compacted sodium bentonite for isolating rock-deposited radioactive waste products," *Nuclear technology*, vol. 45, no. 2, pp. 153-157, 1979.
- [2] M. V. Villar and A. Lloret, "Influence of dry density and water content on the swelling of a compacted bentonite," *Applied Clay Science*, vol. 39, no. 1-2, pp. 38-49, 2008.
- [3] V. Chertkov and I. Ravina, "Tortuosity of crack networks in swelling clay soils," *Soil Science Society of America Journal*, vol. 63, no. 6, pp. 1523-1530, 1999.
- [4] P. Hallett and T. Newson, "Describing soil crack formation using elastic-plastic fracture mechanics," *European Journal of Soil Science*, vol. 56, no. 1, pp. 31-38, 2005.
- [5] S. S. Boynton and D. E. Daniel, "Hydraulic conductivity tests on compacted clay," *Journal of Geotechnical Engineering*, vol. 111, no. 4, pp. 465-478, 1985.
- [6] B. A. Albrecht and C. H. Benson, "Effect of desiccation on compacted natural clays," *Journal of Geotechnical and Geoenvironmental Engineering*, vol. 127, no. 1, pp. 67-75, 2001.
- [7] C. J. Miller, H. Mi, and N. Yesiller, "Experimental analysis of desiccation crack propagation in clay liners 1," *JAWRA Journal of the American Water Resources Association*, vol. 34, no. 3, pp. 677-686, 1998.
- [8] E. Alonso, A. Gens, A. Lloret, and C. Delahaye, "Effect of rain infiltration on the stability of slopes," in *PROCEEDINGS OF THE FIRST INTERNATIONAL CONFERENCE ON UNSATURATED SOILS/UNSAT'95/PARIS/France/6-8 SEPTEMBER 1995. VOLUME 1*, 1995.
- [9] P. Groenevelt and C. Grant, "Analysis of soil shrinkage data," *Soil and Tillage Research*, vol. 79, no. 1, pp. 71-77, 2004.
- [10] K. J. Osinubi and C. M. Nwaiwu, "Desiccation-induced shrinkage in compacted lateritic soils," *Geotechnical and Geological Engineering*, vol. 26, no. 5, pp. 603-611, 2008.
- [11] M. Steinberg, "Geomembranes and the control of expansive soils," 0935803084, 1999.
- [12] C. Vipulanandan and M. Leung, "Treating contaminated, cracked and permeable field clay with grouts," in *Geoenvironment 2000: Characterization, Containment, Remediation, and Performance in Environmental Geotechnics*, 1995: ASCE, pp. 829-843.
- [13] A. Al-Taie, M. M. Disfani, R. Evans, A. Arulrajah, and S. Horpibulsuk, "Swell-shrink cycles of lime stabilized expansive subgrade," *Procedia engineering*, vol. 143, pp. 615-622, 2016.
- [14] G. Omid, T. Prasad, J. Thomas, and K. Brown, "The influence of amendments on the volumetric shrinkage and integrity of compacted clay soils used in landfill liners," *Water, air, and soil pollution*, vol. 86, no. 1-4, pp. 263-274, 1996.
- [15] T. Harianto, S. Hayashi, Y.-J. Du, and D. Suetsugu, "Effects of fiber additives on the desiccation crack behavior of the compacted Akaboku soil as a material for landfill cover barrier," *Water, air, and soil pollution*, vol. 194, no. 1-4, pp. 141-149, 2008.

- [16] C.-S. Tang, B. Shi, Y.-J. Cui, C. Liu, and K. Gu, "Desiccation cracking behavior of polypropylene fiber-reinforced clayey soil," *Canadian Geotechnical Journal*, vol. 49, no. 9, pp. 1088-1101, 2012.
- [17] N. G. Reddy, J. Tahasildar, and B. H. Rao, "Evaluating the influence of additives on swelling characteristics of expansive soils," *International Journal of Geosynthetics and Ground Engineering*, vol. 1, no. 1, p. 7, 2015.
- [18] J. T. DeJong, M. B. Fritzges, and K. Nüsslein, "Microbially induced cementation to control sand response to undrained shear," *Journal of Geotechnical and Geoenvironmental Engineering*, vol. 132, no. 11, pp. 1381-1392, 2006.
- [19] V. Ivanov and J. Chu, "Applications of microorganisms to geotechnical engineering for bioclogging and biocementation of soil in situ," *Reviews in Environmental Science and Bio/Technology*, vol. 7, no. 2, pp. 139-153, 2008.
- [20] N. W. Soon, L. M. Lee, T. C. Khun, and H. S. Ling, "Improvements in engineering properties of soils through microbial-induced calcite precipitation," *KSCE Journal of Civil Engineering*, vol. 17, no. 4, pp. 718-728, 2013.
- [21] N.-J. Jiang, K. Soga, and M. Kuo, "Microbially induced carbonate precipitation for seepage-induced internal erosion control in sand-clay mixtures," *Journal of Geotechnical and Geoenvironmental Engineering*, vol. 143, no. 3, p. 04016100, 2017.
- [22] S. Bang, J. Lippert, U. Yerra, S. Mulukutla, and V. Ramakrishnan, "Microbial calcite, a bio-based smart nanomaterial in concrete remediation," *International Journal of Smart and Nano Materials*, vol. 1, no. 1, pp. 28-39, 2010.
- [23] Y. Fujita *et al.*, "Stimulation of microbial urea hydrolysis in groundwater to enhance calcite precipitation," *Environmental science & technology*, vol. 42, no. 8, pp. 3025-3032, 2008.
- [24] J. T. DeJong, B. M. Mortensen, B. C. Martinez, and D. C. Nelson, "Bio-mediated soil improvement," *Ecological Engineering*, vol. 36, no. 2, pp. 197-210, 2010.
- [25] L. Cheng and M. Shahin, "Assessment of different treatment methods by microbial-induced calcite precipitation for clayey soil improvement," in *Proceedings of the 68th Canadian Geotechnical Conference, 2015*: Canadian Geotechnical Society.
- [26] R. Cardoso, I. Pires, S. O. Duarte, and G. A. Monteiro, "Effects of clay's chemical interactions on biocementation," *Applied Clay Science*, vol. 156, pp. 96-103, 2018.
- [27] M. Li, C. Fang, S. Kawasaki, and V. Achal, "Fly ash incorporated with biocement to improve strength of expansive soil," *Scientific reports*, vol. 8, no. 1, pp. 1-7, 2018.
- [28] Y. Guo, M. Loria, K. Rhoades, and X. Yu, "Effects of Microbial Induced Calcite Precipitation on Bentonite Cracking Remediation," in *IFCEE 2018, 2018*, pp. 135-144.
- [29] H. Kim and H.-K. Lee, "Coal bottom ash in field of civil engineering: A review of advanced applications and environmental considerations," *KSCE Journal of Civil Engineering*, vol. 19, no. 6, pp. 1802-1818, 2015.
- [30] A. Standard, "Standard practice for classification of soils for engineering purposes (Unified Soil Classification System)," *Annual Book of ASTM Standards. ASTM, International West Conshohocken, PA, 2010*.

- [31] T. A. Egloffstein, "Natural bentonites—influence of the ion exchange and partial desiccation on permeability and self-healing capacity of bentonites used in GCLs," *Geotextiles and Geomembranes*, vol. 19, no. 7, pp. 427-444, 2001.
- [32] A. A. Garakani *et al.*, "Effect of road salts on the hydro-mechanical behavior of unsaturated collapsible soils," *Transportation Geotechnics*, vol. 17, pp. 77-90, 2018.
- [33] F. Bell, "Lime stabilization of clay minerals and soils," *Engineering geology*, vol. 42, no. 4, pp. 223-237, 1996.
- [34] O. Manz, "Worldwide production of coal ash and utilization in concrete and other products," *Fuel*, vol. 76, no. 8, pp. 691-696, 1997.
- [35] D. Al-Jeznawi, M. Sanchez, and A. J. Al-Taie, "Using Image Analysis Technique to Study the Effect of Boundary and Environment Conditions on Soil Cracking Mechanism," *Geotechnical and Geological Engineering*, 2020/05/23 2020, doi: 10.1007/s10706-020-01376-5.
- [36] P. C. Prat, A. Ledesma, M. R. Lakshmikantha, and P. C. Prat.
- [37] L.-L. Wang, C.-S. Tang, B. Shi, Y.-J. Cui, G.-Q. Zhang, and I. Hilary, "Nucleation and propagation mechanisms of soil desiccation cracks," *Engineering Geology*, vol. 238, pp. 27-35, 2018.
- [38] M. A. Sutton, J. J. Orteu, and H. Schreier, *Image correlation for shape, motion and deformation measurements: basic concepts, theory and applications*. Springer Science & Business Media, 2009.
- [39] B. Mortensen, M. Haber, J. DeJong, L. Caslake, and D. Nelson, "Effects of environmental factors on microbial induced calcium carbonate precipitation," *Journal of applied microbiology*, vol. 111, no. 2, pp. 338-349, 2011.
- [40] J. Chu, V. Stabnikov, and V. Ivanov, "Microbially induced calcium carbonate precipitation on surface or in the bulk of soil," *Geomicrobiology Journal*, vol. 29, no. 6, pp. 544-549, 2012.
- [41] A. A. QABANY and K. Soga, "Effect of chemical treatment used in MICP on engineering properties of cemented soils," in *Bio-and Chemo-Mechanical Processes in Geotechnical Engineering: Géotechnique Symposium in Print 2013*, 2014: ICE Publishing, pp. 107-115.
- [42] B. Montoya, J. DeJong, and R. Boulanger, "Dynamic response of liquefiable sand improved by microbial-induced calcite precipitation," in *Bio-and Chemo-Mechanical Processes in Geotechnical Engineering: Géotechnique Symposium in Print 2013*, 2014: ICE Publishing, pp. 125-135.
- [43] C. Tang, B. Shi, C. Liu, L. Zhao, and B. Wang, "Influencing factors of geometrical structure of surface shrinkage cracks in clayey soils," *Engineering geology*, vol. 101, no. 3-4, pp. 204-217, 2008.
- [44] P. H. Morris, J. Graham, and D. J. Williams, "Cracking in drying soils," *Canadian Geotechnical Journal*, vol. 29, no. 2, pp. 263-277, 1992.
- [45] C.-S. Tang, Y.-J. Cui, B. Shi, A.-M. Tang, and C. Liu, "Desiccation and cracking behaviour of clay layer from slurry state under wetting–drying cycles," *Geoderma*, vol. 166, no. 1, pp. 111-118, 2011.

- [46] Q. Zhao, L. Li, C. Li, M. Li, F. Amini, and H. Zhang, "Factors affecting improvement of engineering properties of MICP-treated soil catalyzed by bacteria and urease," *Journal of Materials in Civil Engineering*, vol. 26, no. 12, p. 04014094, 2014.
- [47] B. Banagan, B. Wertheim, M. Roth, and L. Caslake, "Microbial strengthening of loose sand," *Letters in applied microbiology*, vol. 51, no. 2, pp. 138-142, 2010.
- [48] J. Li and L. Zhang, "Geometric parameters and REV of a crack network in soil," *Computers and Geotechnics*, vol. 37, no. 4, pp. 466-475, 2010.
- [49] J. Yang *et al.*, "Bioimmobilization of heavy metals in acidic copper mine tailings soil," *Geomicrobiology Journal*, vol. 33, no. 3-4, pp. 261-266, 2016.
- [50] V. Achal, X. Pan, D. Zhang, and Q. Fu, "Bioremediation of Pb-contaminated soil based on microbially induced calcite precipitation," *J Microbiol Biotechnol*, vol. 22, no. 2, pp. 244-7, 2012.
- [51] N. Cristelo, S. Glendinning, T. Miranda, D. Oliveira, and R. Silva, "Soil stabilisation using alkaline activation of fly ash for self compacting rammed earth construction," *Construction and building materials*, vol. 36, pp. 727-735, 2012.
- [52] H. J. Vogel, H. Hoffmann, and K. Roth, "Studies of crack dynamics in clay soil," *Geoderma*, vol. 125, no. 3, pp. 203-211, 2005/04/01/ 2005, doi: <http://dx.doi.org/10.1016/j.geoderma.2004.07.009>.
- [53] C. J. Miller and S. Rifai, "Fiber reinforcement for waste containment soil liners," *Journal of Environmental Engineering*, vol. 130, no. 8, pp. 891-895, 2004.
- [54] H. Peron, L. Laloui, T. Hueckel, and L. B. Hu, "Desiccation cracking of soils," *European Journal of Environmental and Civil Engineering*, vol. 13, no. 7-8, pp. 869-888, 2009 2009, doi: 10.3166/ejece.13.869-888.
- [55] M.-J. Cui, J.-J. Zheng, R.-J. Zhang, H.-J. Lai, and J. Zhang, "Influence of cementation level on the strength behaviour of bio-cemented sand," *Acta Geotechnica*, vol. 12, no. 5, pp. 971-986, 2017.
- [56] B. Koohbor, S. Ravindran, and A. Kidane, "Experimental determination of Representative Volume Element (RVE) size in woven composites," *Optics and Lasers in Engineering*, vol. 90, pp. 59-71, 2017.
- [57] M. A. Sutton, J. H. Yan, V. Tiwari, H. Schreier, and J.-J. Orteu, "The effect of out-of-plane motion on 2D and 3D digital image correlation measurements," *Optics and Lasers in Engineering*, vol. 46, no. 10, pp. 746-757, 2008.